# CHARACTERIZING STRAIN IN THE PROXIMAL RAT TIBIA DURING ELECTRICAL MUSCLE STIMULATION

A Thesis

by

BRENT ARON VYVIAL

Submitted to the Office of Graduate Studies of
Texas A&M University
in partial fulfillment of the requirements for the degree of

MASTER OF SCIENCE

May 2006

Major Subject: Mechanical Engineering

# CHARACTERIZING STRAIN IN THE PROXIMAL RAT TIBIA DURING ELECTRICAL MUSCLE STIMULATION

A Thesis

by

BRENT ARON VYVIAL

Submitted to the Office of Graduate Studies of
Texas A&M University
in partial fulfillment of the requirements for the degree of

MASTER OF SCIENCE

Approved by:

| | |
|---|---|
| Co-Chairs of Committee, | Harry A. Hogan |
| | Susan A. Bloomfield |
| Committee Member, | Xin-Lin Gao |
| Head of Department, | Dennis O'Neal |

May 2006

Major Subject: Mechanical Engineering

# ABSTRACT

Characterizing Strain in the Proximal Rat Tibia During Electrical Muscle Stimulation.

(May 2006)

Brent Aron Vyvial, B.S., Texas A&M University

Co-Chairs of Advisory Committee: Dr. Harry A. Hogan
Dr. Susan A. Bloomfield

Hindlimb unloading is a widely used model for studying the effects of microgravity on a skeleton. Hindlimb unloading produces a marked loss in bone due to increased osteoclast activity. Electrical muscle stimulation is being investigated as a simulated resistive exercise countermeasure to attenuate this bone loss. I sought to determine the relationship between strain measured at the antero-medial aspect of the proximal diaphysis of tibia and plantar-flexor torque measured at the ankle during electrical muscle stimulation as an exercise countermeasure for hindlimb unloading in rats. A mathematical relationship between strain and torque was established for the exercise during a 28 day period of hindlimb unloading. The strain generated during the exercise protocol is sufficient to attenuate bone loss caused by hindlimb unloading. Twelve six-month old Sprague-Dawley rats were implanted with uni-axial strain gages in vivo on the antero-medial aspect of the proximal diaphysis of the left tibia. Strain and torque were measured during electrical muscle stimulation for three time points during hindlimb unloading (Day 0 (n=3), Day 7 (n=3), Day 21 (n=3)). Peak strain decreased from 1,100 μstrain at the beginning of the study to 660 μstrain after 21 days of hindlimb unloading and muscle stimulation. The peak strain rate measured during muscle stimulation was 10,350 μstrain/second at the beginning and decreased to 6,670 μstrain/second after 21 days. The changes in strain are not significant, but the underlying trend in strain values may indicate an increase in bone formation due to the electrical muscle stimulation countermeasure. A mathematical model that relates measured strain to peak eccentric torque during muscle stimulation was created to

facilitate estimation of strain for future studies of electrical muscle stimulation during hindlimb unloading.

# ACKNOWLEDGMENTS

I would like to thank all those persons who have contributed to the completion of this work. In particular, I would like to thank Dr. Harry Hogan for his guidance and support throughout the course of my research. I greatly appreciate the time and effort he has contributed throughout my years of study with him. I would also like to thank Justin Alcorn for his assistance during strain gage surgeries along with other animal care duties and Jan Stallone for teaching me all of the necessary animal procedures. I would like to thank Dr. Susan Bloomfield and Dr. Xin-Lin Gao for serving on my committee. And finally, I would like to thank my family for their support and encouragement throughout my entire college career.

TABLE OF CONTENTS

Page

Page

# LIST OF FIGURES

Page

Page

Page

# LIST OF TABLES

Page

# 1. INTRODUCTION

## 1.1 Motivation and Rationale

The bones of the human skeletal system are constantly undergoing changes to their geometry and composition through the process of remodeling. Through remodeling, old bone is resorbed by osteoclast cells and new bone is formed by osteoblasts. The remodeling process is controlled by genetics, the endocrine system, and external factors. The primary external factor for remodeling is external mechanical loading. External loading of bones is necessary for new bone formation, and during long periods of disuse the balance of remodeling shifts from formation to resorption [(1)]. This shift in the balance of the remodeling process causes a loss of bone in normally weight bearing bones while in microgravity. Therefore, various countermeasures have been considered as methods to attenuate the bone loss caused by microgravity. Countermeasures that have been considered include aerobic and resistive exercise as well as anti-resorptive drugs. While anti-resorptive drugs may effectively attenuate bone loss in microgravity, other effects of the drugs have not been thoroughly examined. This leaves exercise as the most likely countermeasure for bone loss in microgravity. Aerobic and resistance exercise are both beneficial to multiple systems including as muscle, skeletal and neuromotor systems. However, resistive exercise is generally more beneficial to bone than aerobic exercise.

## 1.2 Objectives

Electrical muscle stimulation is being investigated as a simulated resistive exercise countermeasure for hindlimb unloaded rats. Hindlimb unloading is a widely accepted method for simulating microgravity in ground-based scientific studies.

---

This thesis follows the style of the *Journal of Bone and Mineral Research*.

The muscle stimulation protocol of interest in this study uses thin wire electrodes to stimulate the sciatic nerve and contract the major muscles below the knee. The foot is attached to a footplate on the shaft of a servomotor which measures torque applied to the ankle by the muscles. The torque applied to the ankle is used to quantify muscle exertion during the exercise.

The strain during muscle stimulation will be characterized by determining measures of strain magnitude and strain rate from strain gages applied directly to the bone surface. Strains will be characterized at various time points during a period of hindlimb unloading accompanied by muscle stimulation as a potential countermeasure. This will permit assessment of potential changes in strain characteristics as muscle and bone may change. Since the efficacy of the muscle stimulation protocol as a countermeasure is unknown, it is possible that muscle and bone may change during the 28 day study period. A mathematical relationship will be sought between measured torque and observed strain parameters for electrical muscle stimulation at different time points during hindlimb suspension. These relationships will be used to provide guidance and insight into the nature of the strains generated, and their osteogenic potential, at various levels of muscle stimulation without implanting strain gages in the animal.

A companion study to this work is being conducted simultaneously to comprehensively investigate the efficacy of this muscle stimulation protocol as a countermeasure during 28 days of hindlimb unloading. A pertinent question relevant to such studies is whether the muscle torque-bone strain relationships are affected by hindlimb unloading coupled with electrical muscle stimulation. The purpose of the current study is to address the following questions:

1. What is the relationship between ankle torque measured during muscle stimulation and the strain characteristics at the antero-medial aspect of the proximal diaphysis of the tibia?

2. Does the relationship between ankle torque and bone strain change over time when electrical muscle stimulation is used as a countermeasure to hindlimb unloading in rats?

As stated previously, the answers to these questions will provide important input and insight for broader countermeasure studies especially in defining more precisely the magnitude of loading on the skeleton. It should be emphasized, however, that the questions addressed in this study are only relevant for cases utilizing the muscle stimulation protocol as an exercise countermeasure for hindlimb unloaded rats.

# 2. BACKGROUND

## 2.1 Bone Structure

The long bones of the skeleton are composed of two classifications of bone, trabecular (cancellous) bone and cortical bone. Cortical bone makes up the outer shell of long bones and provides the majority of structural rigidity for the bone. Cortical bone is made of compact, concentric layers of bone. Trabecular bone consists of a network of platelets and is found near the ends of long bones. Trabecular bone provides energy absorption for the bone. These types of bone can be seen in Figure 1. The diaphysis region is composed completely of cortical bone with a marrow cavity through the center. The metaphysis of the bone is composed of a shell of cortical bone that is thinner than that of the diaphysis and an inner region of trabecular bone. The epiphysis, which is the very end of the bone, also consists of a cortical shell with an inner region of trabecular bone, which can be seen in Figure 1 [(2)].

## 2.2 Bone Remodeling

Bone is constantly undergoing changes throughout the skeletal system through modeling and remodeling processes. During remodeling, old and hypermineralized bone is replaced by new bone. In cortical bone the old bone is replaced at the endosteal and periosteal surfaces of the cortical bone. For cancellous bone, the old bone is removed and is replaced on the surface of the trabeculae. These types of remodeling occur constantly throughout the entire skeletal system to maintain the structural integrity of the bones in the system. During modeling, bone is removed in some areas and formed on other surfaces of the bone. The architecture of the bone is changed by resorption in areas and growth by apposition in others.

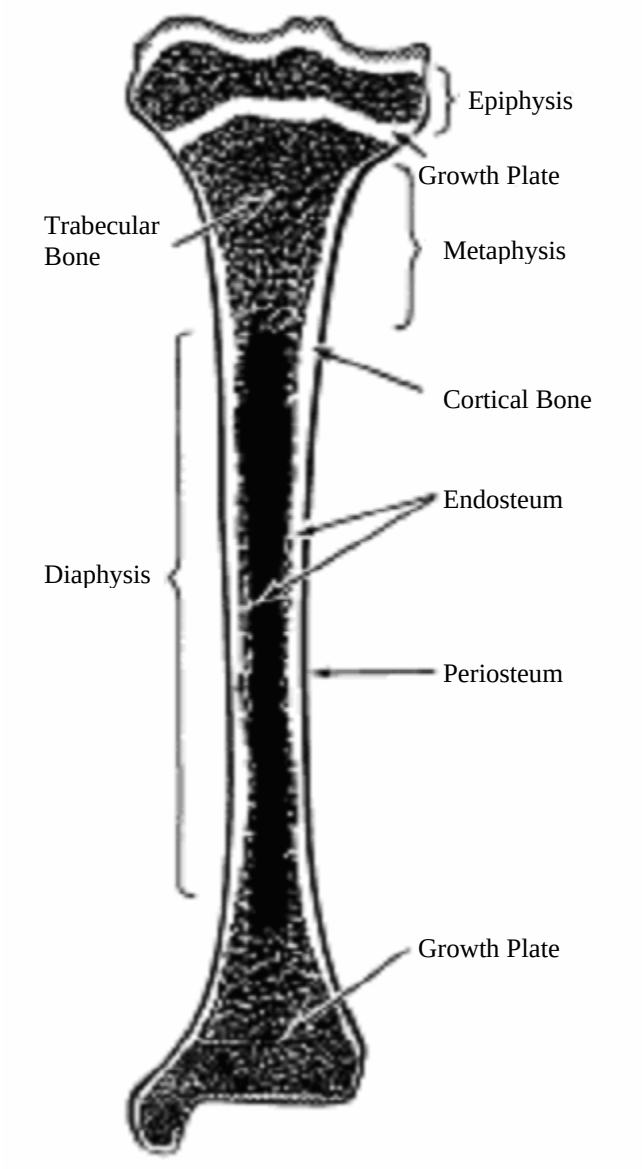


**Figure 1.** Diagram of a human tibia [(2)].

This modeling typically occurs when the external stimulus applied to the bone is changed. When new loads are applied, the bones are remodeled in order to change the cross-section of the bone in order to better accommodate the new loading conditions. For instance, when a fracture heals and the shape of the bone differs from the original shape, the bone is then remodeled in order to return it to the original shape. Bone is formed in areas with increased compressive stress and resorbed in areas of increased tensile stress [(3)].

The basic types of bone cells involved in remodeling are osteoblasts, which form new bone, and osteoclasts, which resorb bone away. When the process of bone remodeling takes place, osteoclasts are signaled by osteoblasts and move to the area, attaching to the surface of the bone. The osteoclasts then begin to produce proteolytic enzymes and hydrogen ions under the ruffled border of the cell [(2)]. The enzymes and hydrogen ions begin breaking down the mineralized bone matrix creating a resorption lacuna. The osteoclasts then reverse and move out of the resorption lacuna. After the osteoclasts leave, osteoblasts move into the lacuna and begin to secrete a matrix of unmineralized collagen called osteoid. The osteoid is then mineralized under the control of the osteoblasts to form new bone. Osteoblasts that stay behind as bone is formed are known as osteocytes. They are encapsulated in cavities known as lacunae, which are interconnected to one another through a network of passages called canaliculi [(2)]. It is believed that osteocytes are the primary method for mechanical transduction [(2)].

## 2.3 Mechanotransduction

Mechanotransduction describes the ability of bone to adapt to changes in mechanical stimulus. Bone responds to mechanical loading by adapting its geometry to provide optimal mechanical function [(4)]. Bone adaptation is dependent on the peak strain level applied to the bone (Figure 2).

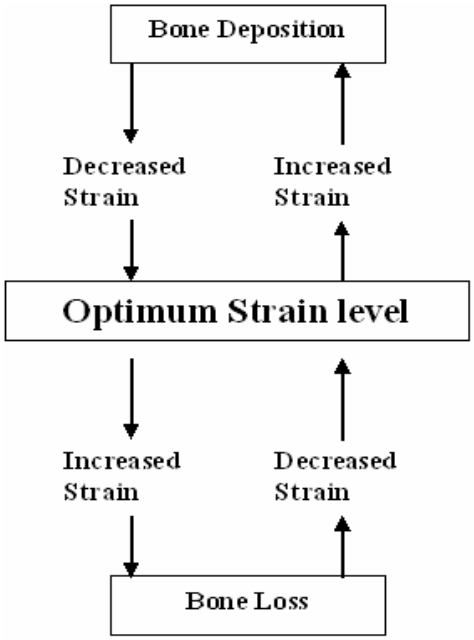


**Figure 2.** Feedback model of bone adaptation [(1)].

Bone adapts in order to maintain strain levels in a physiological range, and strain levels below this range cause increased resorption while strains above the range cause increased formation [(4)]. Bone structure does not necessarily change simply to minimize strain but also to confine strains to a more predictable pattern [(1)].

An important signaling mechanism for bone formation is fluid shear stress (FSS) which is induced by strain gradients in the bone. FSS across the cell membrane of osteocytes causes them to signal osteoblast cells to begin bone formation. The osteocyte cells trigger bone formation by expressing various genes and growth factors necessary for formation. Cultured bone cells have been stimulated by applied fluid shear stress [(5)].

## 2.4 Osteogenic Thresholds

Increases in mechanical loading above that normally applied to bone can lead to new bone formation (osteogenesis). Normal loading of long bones during activities such as walking or running, in both humans and rats, induces bending loads in the tibia and femur due to their curvature. The anterior (front) of the bone is in tension while the

posterior (back) of the bone is in compression. The strain gradients created by mechanical loading create a pressure gradient across the bone. This pressure gradient induces fluid flow through the canaliculi and the fluid shear stress causes osteocytes to trigger remodeling [5]. The level of strain seen in normal activities is enough to maintain the structural integrity of the bone through remodeling. However, strain magnitudes higher than the normally experienced physiological levels can lead to osteogenesis. Controlled studies aimed at understanding these processes in live animals are almost exclusively limited to animal studies. The focus is on rats, which are most relevant to the current research.

### *2.4.1 Methods of Studying Mechanical Loading of Rodents In Vivo*

One model used to study mechanical loading of rodents is the four-point bender. Load is externally applied through two pads on the medial side of the tibia with the lateral side of the tibia resting on another two pads (Figure 3) [6]. The four-point bender creates a region of constant bending moment between the loading pads. This method is more desirable than a three-point bender in which the bending moment varies along the length of the bone.

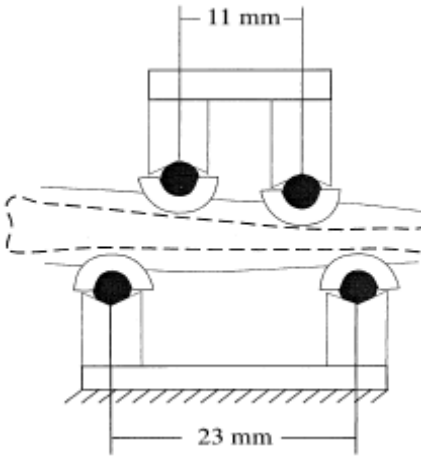


**Figure 3.** Diagram of four-point bender [6].

Another model for studying mechanical loading of rodents is the ulna loader. The ulna loader applies load to the rat ulna through the flexed carpus and holds the olecranon (Figure 4) [7]. This method is more physiological than the four-point bender because the curve of the ulna creates bending strains similar to normal ambulation. Therefore, this method of loading better approximates physiological loading conditions than the four-point bender model.

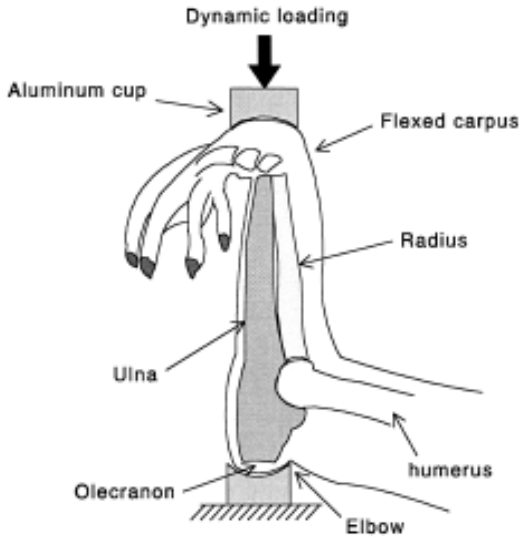


**Figure 4.** Diagram of the ulna loader [7].

A method of applying load to the tibia in mice loads the tibia axially in the same manner as the ulna loader [8]. This external loading model more closely resembles physiological loading because the tibia is loaded in the same direction. The tibia is loaded by padded cups similar to those used in the ulna loader (Figure 5).

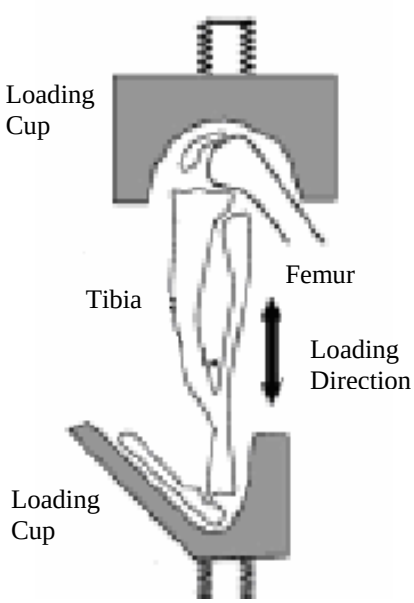


**Figure 5.** Diagram of the axial tibia loader [8].

*2.4.2 Strain Magnitude*

From studies using a tibia four-point bender, the minimum strain magnitude that will induce an osteogenic response in cortical bone at the midshaft of the rat tibia is 1,000 μstrain [9]. The minimum strain magnitude for osteogenesis also varies with location along the shaft of the bone. From ulna loading, the osteogenic threshold is 2284 μstrain at the midshaft while the thresholds at locations 3mm proximal and distal to the midshaft are 1343 and 3074 μstrain, respectively [7]. With axial loading of the tibia in mice, strain on the medial aspect at the midshaft of approximately 1500 μstrain produced an increase in cortical bone area along the length of the tibia [8]. A diagram of approximate strain levels and the effects on osteogenesis is shown in Figure 6. It should also be noted that the strain levels to generate an osteogenic response must be dynamic; static strain does not induce new bone formation [8].

In a study of rats walking with a gait frequency of 1.3 Hz on a treadmill with implanted strain gages, peak strain at the mid-diaphysis was 375 μstrain [10]. When the gait frequency was increased to 1.8 and 2.1 Hz, the peak strain increased to 500 and 550

μstrain respectively [10]. For normally ambulating mice, strain on the medial aspect of the midshaft of the tibia was 300 μstrain [8]. During a 30 cm jump, the strain at the same location in the mice was 600 μstrain [8]. These strain levels during walking, running, and jumping are within the physiological strain window described by Turner [4]. Strain levels in bone are similar between rats and humans. Strain at the midshaft of the human tibia during walking on a level surface was 544 μstrain, which is close to the level seen in rats on a treadmill [10, 11]. For a running human, strain at the midshaft of the tibia increased to 968 μstrain [11].

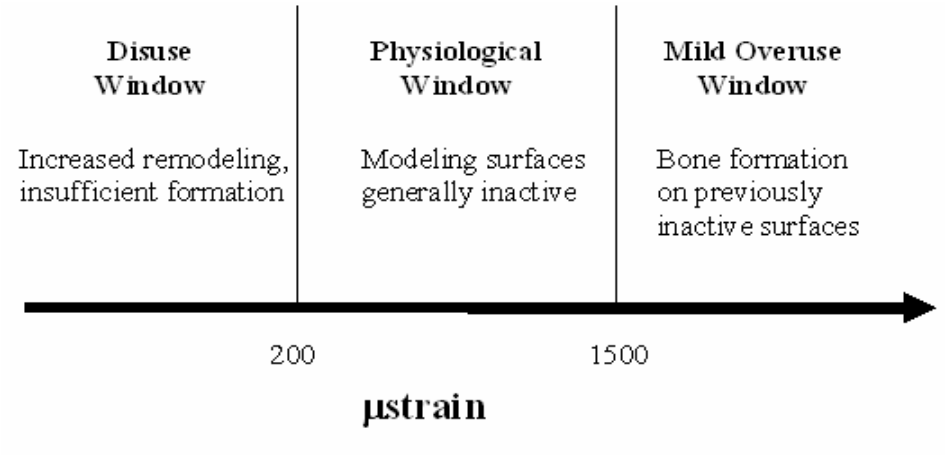


**Figure 6.** Diagram of osteogenic strain magnitudes [4].

### *2.4.3 Loading Frequency, Number of Cycles and Strain Rate*

Along with strain gradients, repetitive loading of bone is necessary to generate an osteogenic response. As loading frequency increases, fluid flow around osteocytes is increased [5]. However, at higher loading frequencies, osteocytes become less sensitive to fluid flow because the stiffness of the cells increases [5]. For lower strain magnitudes, the loading frequency must be increased in order to induce osteogenesis. When the number of cycles is kept constant, the strain threshold for osteogenesis decreases from 1,200 to 100 μstrain when the loading frequency is increased from 1 to 30 Hz [9].

Along with strain magnitude and loading frequency, the number of load cycles is an important factor for osteogenesis. The effect of cycle number on osteogenesis increases as the strain magnitude decreases [9]. For a strain magnitude of 800 μstrain the number of cycles required for osteogenesis is 400 cycles per day, but for a strain magnitude of 1000 μstrain the required cycle number is 120 cycles per day [9].

Rest inserted in between loading sessions can cause bone formation with high loading frequencies. With increased loading frequencies, the fluid flow around osteocytes does not have time to recover from damping effects which negates the flow in the lacuna and canaliculi [12]. After the first few loading cycles the shear stress experienced by osteocytes is greatly reduced due to the lack of fluid flow which reduces the potential for bone formation [12]. By inserting a rest period in between loading cycles, the fluid around the osteocytes is allowed to return to its resting state thereby maximizing the effects of the loading cycles for osteogenesis.

Perhaps the most influential factor for new bone formation is strain rate. Fluid shear stress on cell membranes is proportional to applied strain rate. At higher strain rates, fluid shear stress is increased which in turn increases osteogenic potential [5]. In a four-point bending study in rats, a strain rate of 4,800 μstrain/second triggered a bone response with 36 loading cycles [9]. For 400 loading cycles, a strain rate as low as 3,200 μstrain/second was necessary to produce a bone response [9]. In another four-point bending study where load was held constant and strain rate was varied, increases in strain rate led to an increase in bone formation [13]. Strain rate is believed to be the primary driving force behind mechanically induced bone formation [13].

## 2.5 Effect of Microgravity on Bone

### *2.5.1 Bone Loss in Humans*

Long term spaceflight (> 1 month) can lead to a decrease in bone mass even in healthy individuals. On the International Space Station, astronauts lost 1.06% bone mineral density (average BMD) per month in the hip [14]. Long term spaceflight was once believed to cause osteoporosis, but has since been shown to cause bone loss only in

weight bearing bones such as the tibia and femur which does not constitute true systematic osteoporosis [15]. Bone loss in microgravity occurs first in trabecular bone and after longer periods of time bone loss occurs in both trabecular and cortical bone. During the first month aboard the MIR space station bone loss in cosmonauts was observed only in trabecular bone (2.27%) in the tibia, while after six months bone loss was observed in both trabecular bone (4.5%) and cortical bone (2.9%) in the tibia when measured by peripheral QCT [15].

### *2.5.2 Bone Loss in Hind-Limb Suspended Rat Model*

Animal models are commonly used to simulate the weightlessness experienced in microgravity. An effective animal model for microgravity is the hindlimb suspended rat. The animals are suspended from a wire at the top of the cage by the tail at a $30^{o}$ head-down angle in order to remove weight from the hindlimbs of the animal, while allowing the animal to ambulate on its front limbs. Hindlimb suspension of rats also creates a cephalic fluid shift like the shifts observed during spaceflight [16]. In mature rats, the bone formation rate on the periosteal surface drastically decreased during the final week of the 28-day hindlimb unloading period [17].

### *2.5.3 Bone Loss in Microgravity Rat Model*

The change in bone formation in rats in microgravity is different than that of hindlimb suspended rats. Changes in trabecular bone in the tibial proximal metaphysis are similar between rats in microgravity and hindlimb unloaded rats for a 7-day period of time; however, greater bone loss was observed in the rats in microgravity [18]. While bone responses may vary between microgravity and hindlimb unloaded animal models, hindlimb unloading is a widely accepted model for microgravity due to the similar if not identical bone effects and to the daunting logistics of studying rats in a weightless environment [16]. Hindlimb unloading mimics many of the same effects observed in rats in microgravity [16].

## 2.6 Electrical Muscle Stimulation

Electrical muscle stimulation is a method of simulating resistive exercise that is being investigated as a countermeasure for hindlimb unloading in rats. Electrical muscle stimulation uses electrodes to stimulate the sciatic nerve and contract the muscles in the leg. The stimulation frequency controls the intensity of the muscle contractions during stimulation. One advantage of electrical muscle stimulation is the loading is physiological instead of applying load externally with bending or compression devices without concurrent muscle contractions. Also, by varying the stimulation frequency, the muscle load level can be adjusted over a range of intensities and can be used to simulate resistive exercise levels. Another benefit of stimulated muscle contractions is the ability to assess bone and muscle together as well as cortical and cancellous bone since the tibia contains both types of bone. One disadvantage of using electrical muscle stimulation is that the animal is anesthetized during the exercise. Further, since the exercise is involuntary, the model only simulates the mechanical effect of muscle contractions and not the integrative response to exercise, which includes neural and hormonal factors.

## 2.7 In Vivo Loading During Hindlimb Unloading

In hindlimb unloaded rats where muscles were chronically stimulated while the rat was suspended, stimulation frequencies as low as 10 Hz improved trabecular bone formation in the tibia but did not completely counteract bone loss from hindlimb unloading [19]. Higher frequencies of 50 and 100 Hz had more of an effect on bone formation due to the higher loads applied to the bone during stimulation [20]. During these electrical muscle stimulation protocols, all of the muscles in the hind leg were contracted with no constraint of movement for the entire leg and contractions were stimulated 2,880 times per day for 10 consecutive days [20]. Higher muscle loads can be applied by constraining movement at the knee and the ankle joint and allowing muscles to act against a lever; therefore, the same beneficial effect in the tibia may be observed with a protocol consisting of fewer daily contractions with higher applied loads to the bone.

In hindlimb unloaded rats which underwent electrical stimulation using surface electrodes with a stimulation frequency of 30 Hz, strain amplitude at the antero-medial surface of the proximal diaphysis was 200 μstrain [21]. When these stimulations are applied for 10 minutes per day during a four week hindlimb unloading period, bone formation increases over unloaded controls but not to the level of weightbearing cage controls [21]. A larger increase in bone formation may be possible using percutaneous electrodes to directly stimulate nerves innervating hindlimb muscles and a higher stimulation frequency.

Another method of simulating resistive exercise utilizes a flywheel to provide resistance. This model requires the rat to leap forward to overcome the inertia of the flywheel and the spinning flywheel then returns the rat to the starting position, thus providing an eccentric component to the exercise [22]. A flywheel protocol using 50 repetitions per day, 3 days per week, effectively mitigates loss of bone mineral density in the distal femur in adult rats subjected to 28 days of hindlimb unloading [22]. Since the exercise is voluntary, the level of intensity for the exercise may not achieve the intensity of resistive exercise as practiced by highly motivated humans. The advantage of this model is that it does simulate the integrated systemic response to exercise, since it is performed voluntarily by the conscious animal.

## 2.8 Strain Gage Theory

The strain gages used in this study are 120 Ω resistance strain gages (EA-06-015SE-120, Measurements Group, NC). The electrical resistance strain gage utilizes the linear dependence of resistance on the geometry of the conductor. The gages used in this study consisted of a polymide backing with a metallic foil grid as shown in Figure 7.

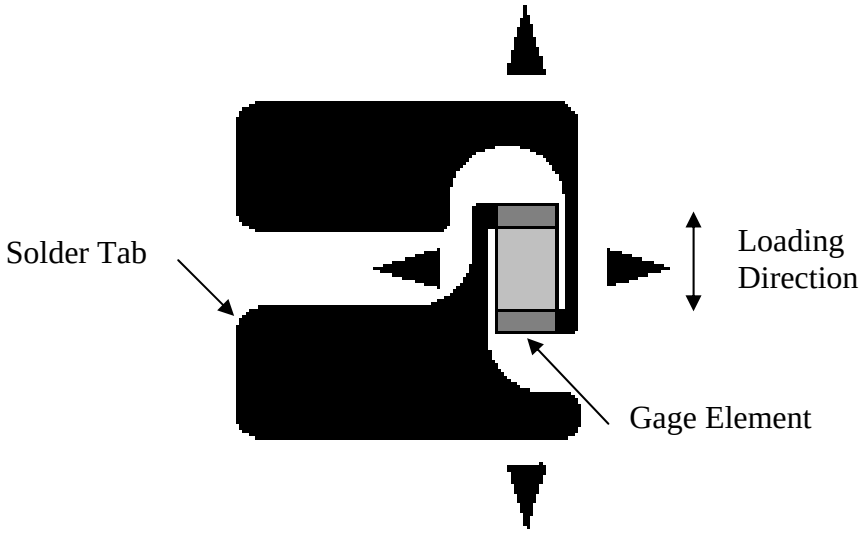


**Figure 7.** Diagram of model EA-06-015SE-120 strain gage [23].

As the gage element is stretched, the resistance of the gage increases due to a reduction in cross-sectional area of the grid elements; however, the change in resistance is too small to measure directly. Therefore, the gage is connected to three known resistors in a Wheatstone Bridge circuit, to which an excitation voltage ($V_{in}$) is applied. The diagram of a Wheatstone Bridge is shown in Figure 8. The strain gage is denoted in the figure as $R_g$.

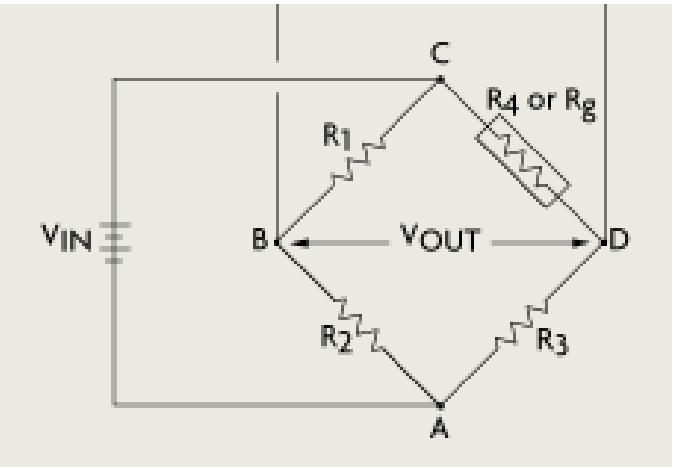


**Figure 8.** Schematic diagram of the Wheatstone bridge circuit [23].

The output voltage ($V_{out}$) from the bridge is measured in millivolts per input volt and reflects the change in resistance of the gage element. The relationship between $V_{out}$, $V_{in}$, and $R_g$ is determined using Equation 1 [23].

$$V_{OUT} = V_{IN} \frac{R_3 R_1 - R_g R_2}{(R_2 + R_3)(R_1 + R_g)} \qquad \text{(Equation 1)}$$

This equation is solved for $R_g$ before and after a load is applied. The difference between the values ($\Delta R_g$) can be related to the strain ($\varepsilon$) as follows:

$$\varepsilon = \frac{\left( \Delta R_g / R_g \right)}{GF}, \qquad \text{(Equation 2)}$$

where $R_g$ is the resistance of the gage before the load is applied [23]. The gage factor (GF) is the change in resistance of the gage per unit of applied strain.

# 3. METHODS AND MATERIALS

## 3.1 Animals

Hindlimb unloaded (HU) animals were studied and compared to baseline animals (BL) tested on Day 0. The time points for strain measurement selected were 7 and 21 days because the majority of muscle atrophy occurs by the 7$^{th}$ day, whereas significant and detectable bone changes do not occur until the final week of hindlimb unloading [17, 24]. Measuring strain on Day 21, which was the beginning of the beginning of the final week of the protocol, generated a torque/strain calibration curve for the final week of muscle stimulation. Strain measurements for Day 0 were taken on a set of baseline animals that required no treatments.

Nine 6-month old male Sprague-Dawley rats were housed in identical cages with a 12-hour light/dark cycle and given food and water ad-libitum. The rats were then randomly assigned to a baseline group (BL, n=3) or one of two hindlimb unloaded groups (HU-7, n=3) and (HU-21, n=3). Only three animals were used for each time point because of the technical challenges in attaching strain gages to the bone surface in live animals. Another factor influencing group size is the large quantity of data collected in multiple waveforms that was analyzed for multiple parameters.

## 3.2 Hindlimb Unloading

For the animals in the HU groups, the rats were suspended using tail harnesses. The rat was first anesthetized using a Ketamine-Metetomidine mixture and the tail was cleaned thoroughly with soap and water and then acetone and allowed to dry. After drying, the tail was sprayed with contact adhesive and allowed to dry. Two pieces of surgical tape were then attached to both sides of the tail along its mid-length using an adhesive (Marine Goop). A hook at the end of the harness was attached to a swivel on a cable stretched across the cage so that the body of the rat was at a 30$^{o}$ angle to the floor of the cage as shown in Figure 9.

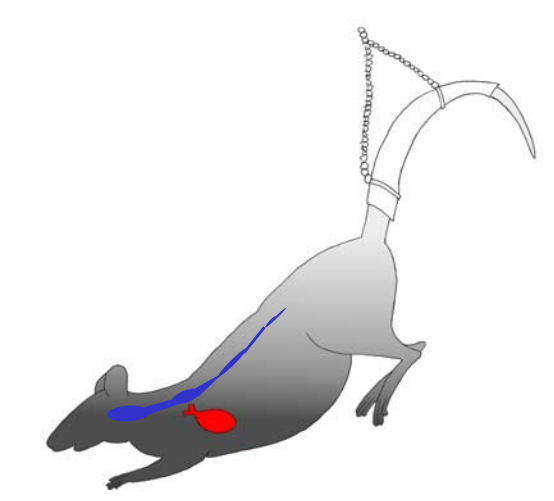

**Figure 9.** Diagram of a hindlimb unloaded rat [17].

The swivel was allowed to travel along the cable so that the rat could ambulate on its front limbs around the entire cage without resting its hindlimbs on the bottom or sides of the cage. The rats were able to eat, drink and groom normally while hindlimb unloaded.

## 3.3 Muscle Stimulation

The hindlimb unloaded groups underwent a muscle stimulation protocol on alternate days, three days/week on the left leg. These exercise sessions consisted of eccentric muscle contractions where the muscles lengthen while they contract. The eccentric muscle contractions were chosen for the exercise protocol because they provide the highest force and appear to maximize the bone response. The rats were anesthetized by Isoflurane inhalation (2%, v/v in air) and stimulations provided by a Grass S48 stimulator and SIU-5 stimulus isolation unit (Grass-Telefactor, RI) were administered with percutaneous Teflon-coated stainless steel fine wire electrodes inserted on either side of the sciatic nerve in the upper leg. Before the electrodes were inserted, a small amount of Teflon coating was removed from the tip of the wire to expose the wire. Since stimulating the sciatic nerve causes all of the muscles to contract, the left knee was clamped at an angle of $90^{o}$ to constrict movement to the lower leg. The

tendons of dorsiflexor muscles were not ablated as in previous studies on sacrifice days due to permanent injury incurred, so the dorsiflexor muscles contribute to the measured ankle torque [25].

Torque generated at the ankle was measured by securing the left hind foot to an aluminum footplate attached to an Aurora Scientific 305B servomotor (Aurora, Ontario, Canada) with the ankle at a $90^o$ angle to the tibia. The ankle angle of $90^o$ was chosen because it is when the plantarflexors are the most active during normal, voluntary ambulation and is approximately halfway between maximum dorsiflexion and plantarflexion angles observed during normal ambulation [25]. The ankle's axis of rotation was in line with the shaft of the servomotor so that the torque measured by the servomotor equaled the torque at the ankle. Electrical pulses applied to the sciatic nerve caused the muscles in the lower leg to contract and plantar-flex the foot while the footplate moved from $20^o$ plantarflexion to $20^o$ dorsiflexion at a rate of $100^o$ per second to induce eccentric contractions of the gastrocnemius, plantaris and soleus muscles. Eccentric torque was recorded using TestPoint software (SuperLogics Inc., MA) sampling at 10 kHz from a KPCI-3108 A/D board (Keithly Instruments, OH). Figure 10 contains a diagram of the muscle stimulation unit illustrating leg position and fine wire electrode placement.

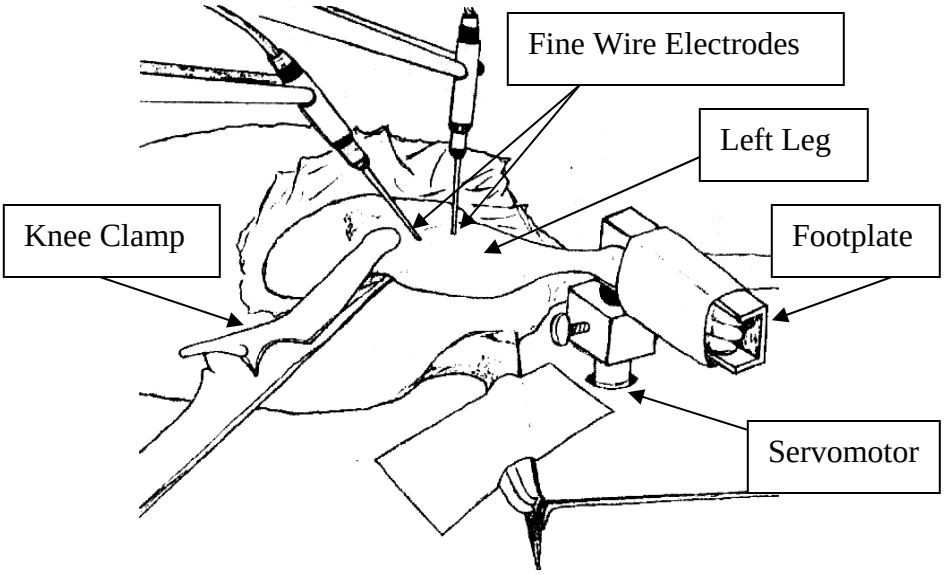


**Figure 10.** Diagram of muscle stimulation unit [26].

Before each exercise session, each animal underwent isometric muscle contractions to optimize the stimulation voltage at 175 Hz and establish a peak isometric torque. Isometric muscle contractions occur when the muscle contracts without any change in length, so the footplate was kept stationary with the ankle at a $90^{o}$ angle. The voltage had to be optimized for each exercise session to account for changes in electrode placement with respect to the sciatic nerve.

For every exercise session, each rat was subjected to single eccentric contractions until 120% of peak isometric torque was reached to determine the stimulation frequency for the exercise session. The exercise sessions consisted of 4 sets of 10, 500ms eccentric contractions with a ten-second rest between contractions and a two-minute rest period between sets.

Strain measurements were collected during eccentric contractions on the sacrifice day for each group. After 3 exercise sessions had been completed, strain measurements during eccentric contractions were taken for the HU-7 group on the day after the final exercise session. The HU-21 group continued the stimulation protocol and after 9 exercise sessions, strain measurements were taken on the day following the final

exercise session. A graphical representation of strain measurement/sacrifice days is shown in Figure 11.

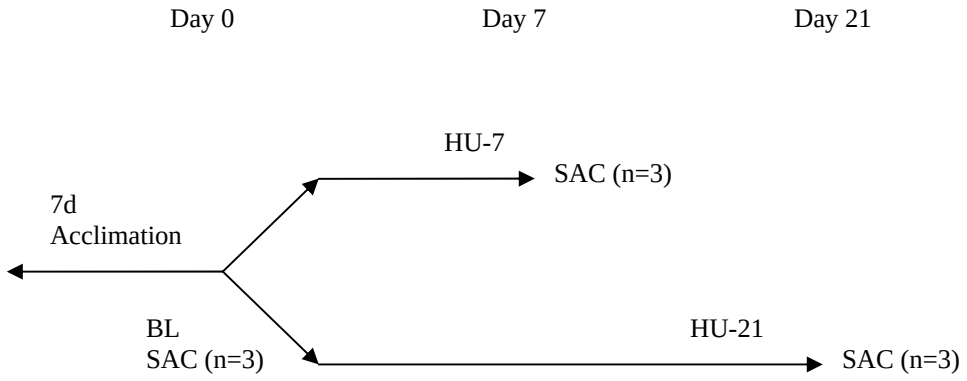


**Figure 11.** Graphical design of experiment (n=9 animals).

3.4 Strain Measurement

To prepare the rats for strain measurements, each rat was anesthetized by Isoflurane inhalation (2.5%, v/v in air) and a small incision made over the medial side of the proximal tibia. The tendon and periosteum were removed to expose the antero-medial surface of the proximal diaphysis of the tibia. This strain gage location was chosen because most changes in bone during hindlimb unloading occur in cancellous bone in the metaphysis [17]. A drop of epinephrine and saline solution on a cotton swab was used to reduce blood flow, by constricting small blood vessels, from the surface of the bone and surrounding tissue. The area was cleaned and dried with isopropyl alcohol and a drop of cyanoacrylate applied to the area. A 120 Ω uni-directional strain gage (EA-06-015SE-120, Measurements Group, NC), which had been sealed with layers of nitrile rubber and polyurethane (Measurements Group, NC), was applied to the bone with pressure for 1 minute. A complete procedure for strain gage implantation is included in Appendix C. The gage was attached to the antero-medial aspect of the

proximal diaphysis of the tibia approximately 11mm from the proximal end of the tibia. The placement of the strain gage on the tibia is shown in contact radiographs (Figure 12) and a photograph (Figure 13). The gage element is too small to be seen in the radiographs, so the most prominent features visible in the radiographs are the solder tabs of the strain gage.

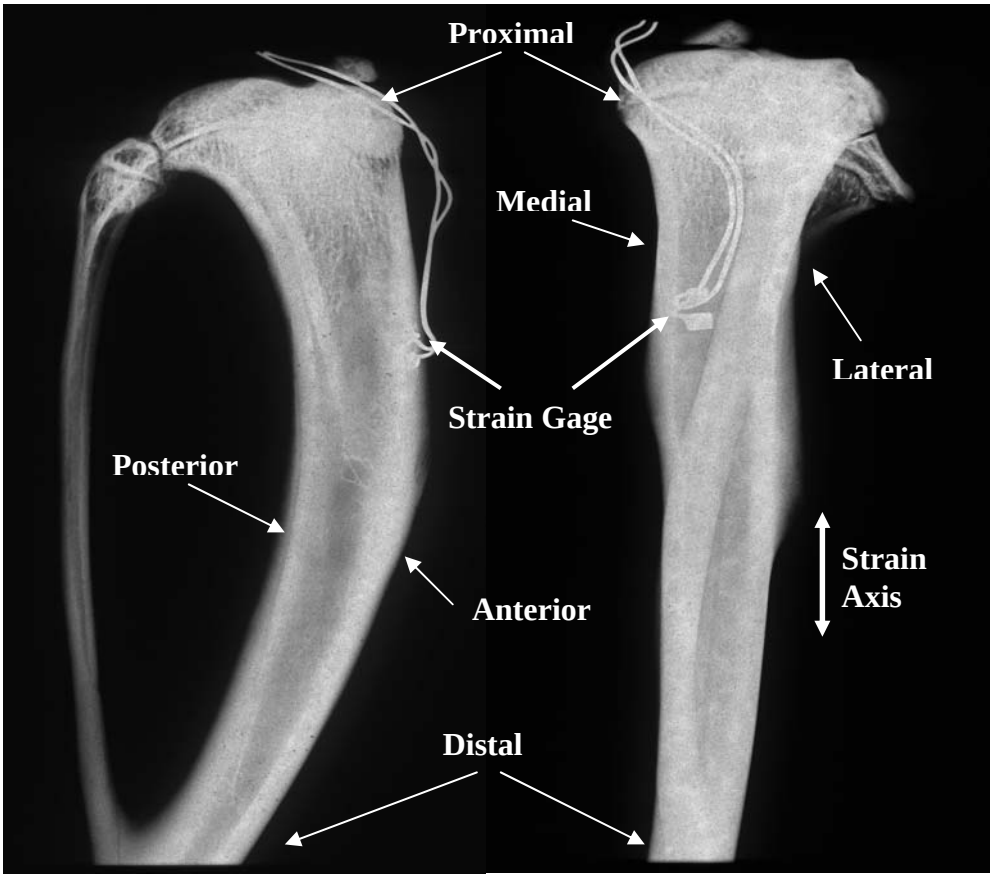


**Figure 12.** Contact radiographs of the sagittal and coronal aspects of a tibia with a strain gage attached.

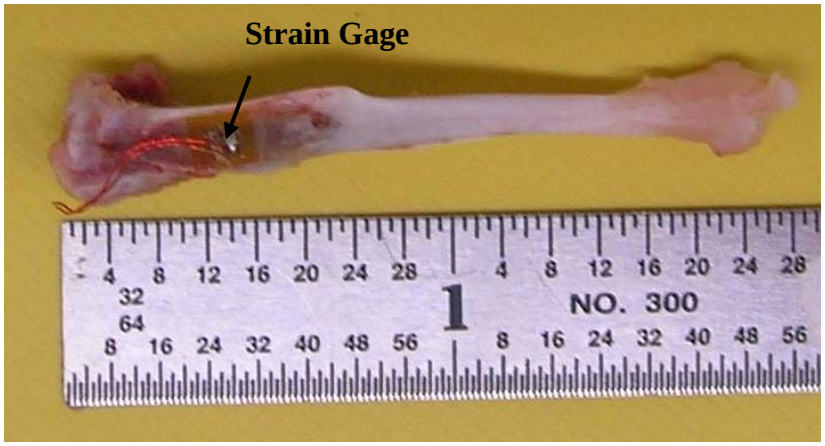


**Figure 13.** Photograph of the antero-medial aspect of a tibia with a strain gage attached.

The lead wires from the gage were attached to a signal conditioner (Model 6100, Measurements Group, NC). After implantation of the strain gage, the rat was positioned in the muscle stimulation device and the gage was zeroed and shunt calibrated with the muscles relaxed. The voltage was optimized and peak isometric torque measured as described previously. Each rat was then subjected to eccentric muscle contractions at stimulation frequencies of 30, 40, 50, 60, 70, and 80 Hz, and strain measurements for each contraction were collected using StrainSmart Software (Measurements Group, NC) sampling at 5 kHz. The large range of stimulation frequencies was chosen to produce a more complete assessment of the relationship between muscle torque and proximal tibia strain, rather than measuring strain only at 120% of peak isometric torque. After strain measurements were taken, the animal was anesthetized and euthanized by decapitation.

## 3.5 Data Analysis

Strain data collected from each animal were trimmed to eliminate unnecessary data before and after the muscle contraction. A strain versus time graph for a single baseline animal is shown in Figure 14 as an example of the recorded strain versus time data.

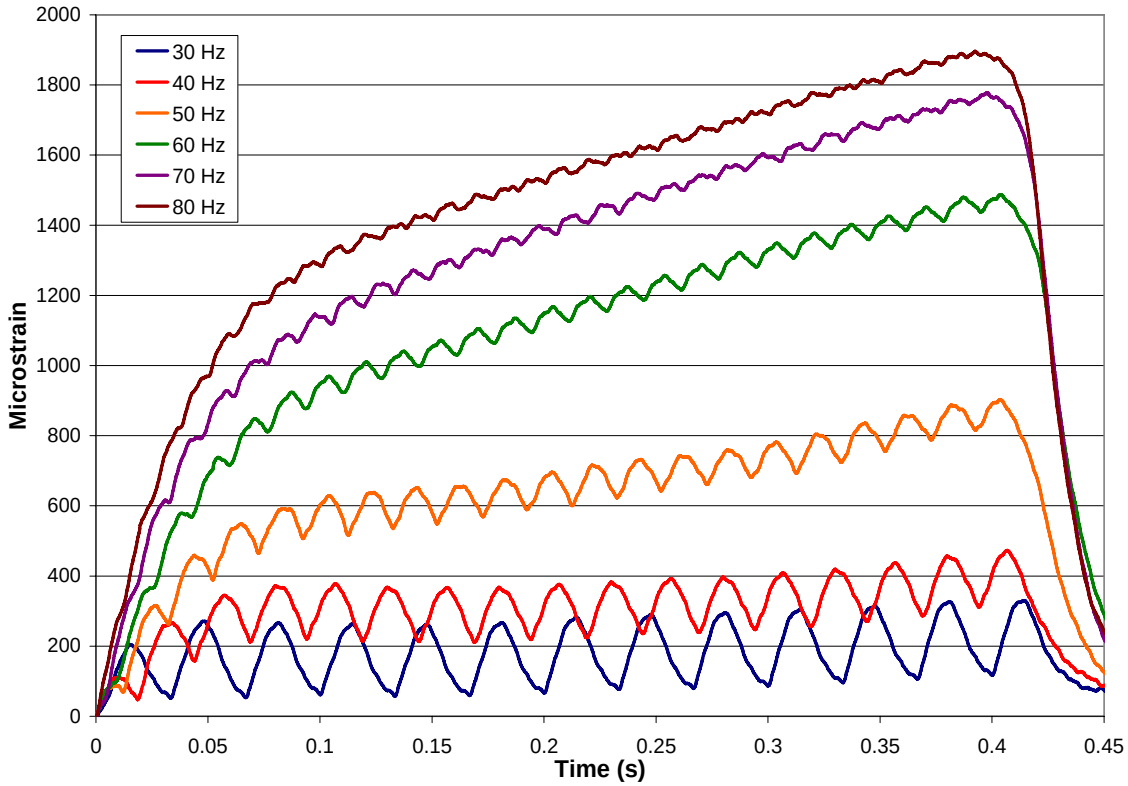


**Figure 14.** Strain vs. time curves for one baseline (BL) animal.

Data for each stimulation frequency were analyzed using Excel (Microsoft) to determine peak strain magnitude, average strain magnitude, initial strain rate and secondary strain rate for the given stimulation frequency. An example of a strain versus time curve with key strain parameters labeled is shown in Figure 15.

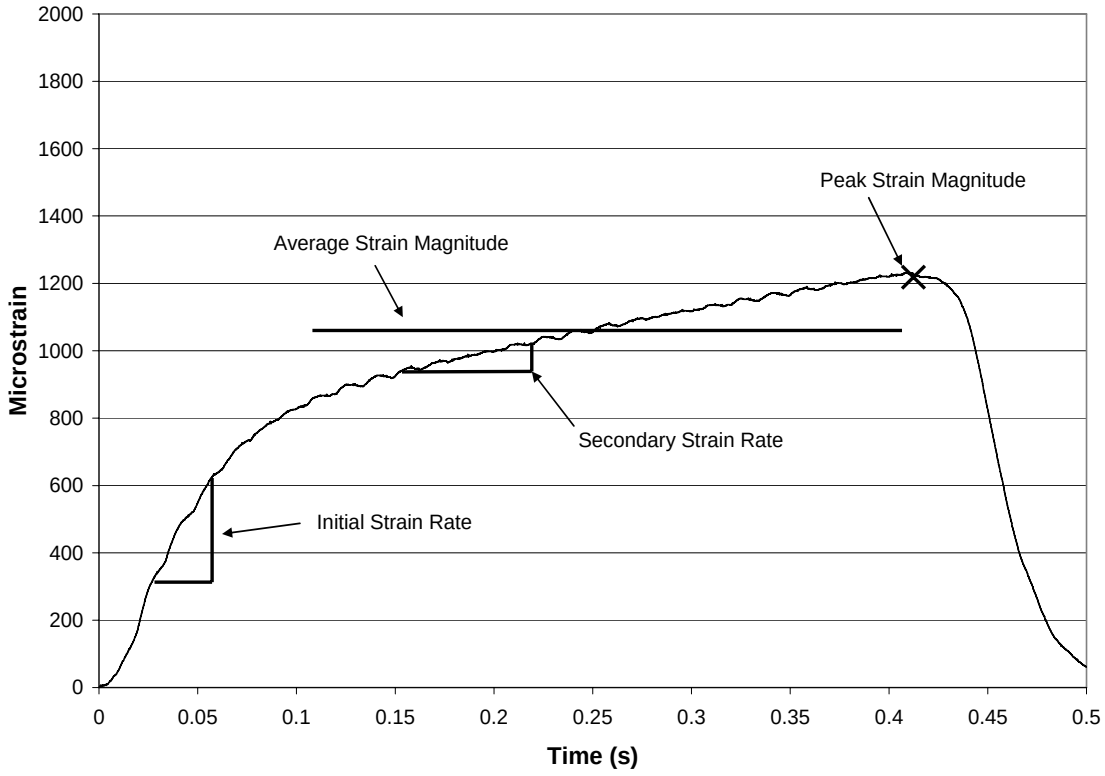


**Figure 15.** Example strain vs. time curve with strain parameters labeled.

Peak strain is the highest strain measured during the contraction, and the average strain values for each contraction were calculated by averaging strain between 0.1 and 0.4 seconds from the start of the contraction. The initial strain rate is the strain rate at the beginning of the contraction. The secondary strain rate for each contraction was calculated by averaging the instantaneous strain rates between 0.1 and 0.4 seconds after the start of the contraction. By averaging the instantaneous strain rates, small muscle twitches were eliminated, and the underlying rate was characterized. The time period between 0.1 and 0.4 seconds from the start of the contraction were chosen because for the majority of the stimulation frequencies, this time period was between the initial rise and final decline in the strain curve.

Each parameter was then plotted against the corresponding absolute or relative (%) peak isometric torque for each group of animals. Linear regression was utilized to

determine relationships between strain parameters and eccentric torque or % peak isometric torque using SigmaStat (Systat Software Inc., CA). The linear regression tool in SigmaStat includes not only the $R^2$ value for the regression, but also the significance of the slopes and intercepts. The torque-strain relationships for each group were then compared to the relationships for the other groups, and a one-way ANOVA was performed using SigmaStat (Systat Software Inc., CA) to determine the significance of any differences in slope and intercept among groups for each parameter.

# 4. RESULTS

## 4.1 Peak Strain

Peak strains for each stimulation frequency were plotted against the eccentric torque at that frequency for each group of animals. As stated previously, strain was measured for 6 stimulation frequencies for each animal, for a total of 18 data points per group (Figure 16).

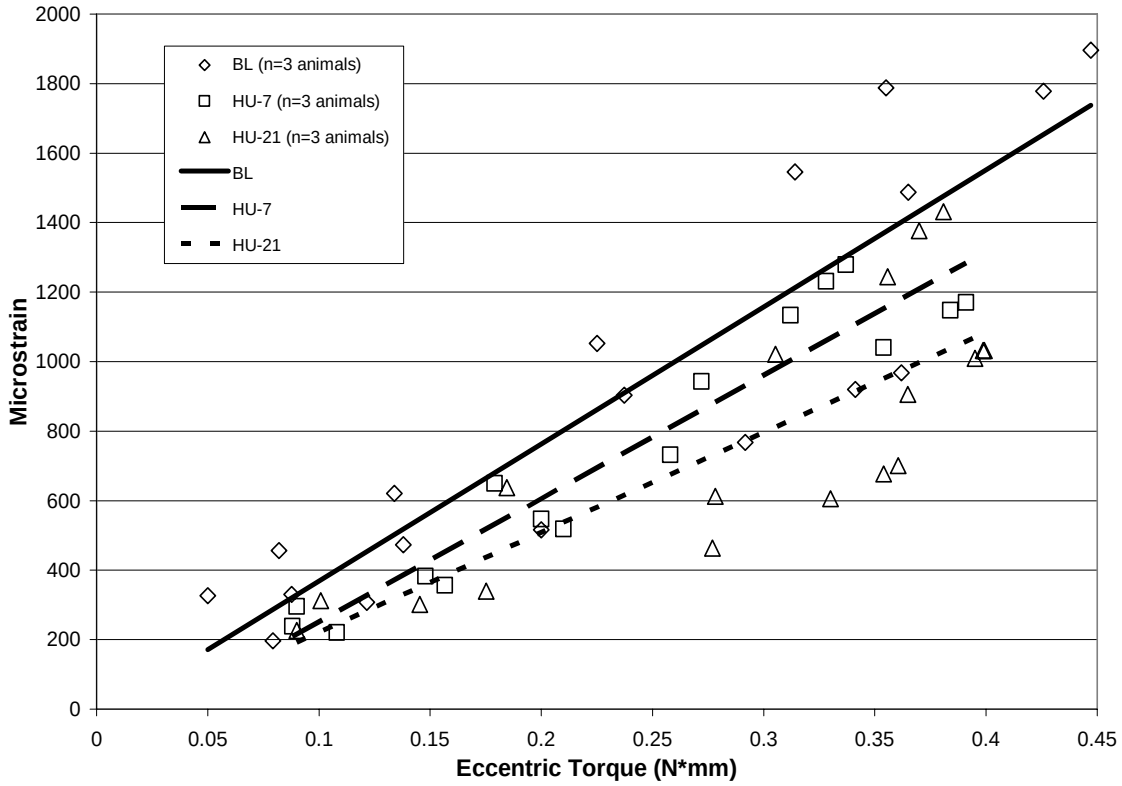


**Figure 16.** The peak strain vs. eccentric torque plot shows a decrease in strain magnitude for a given torque while the slopes remain similar.

The plot contains linear regression lines which establish a mathematical relationship between eccentric torque and peak strain. The slopes of the curves for BL and HU-7

appear to be similar while the HU-21 slope appears to be slightly lower (Table 1). While the peak strain curves trend lower over time, the slopes and intercepts are not significantly different among groups. The intercepts for all three groups are close to the same.

**Table 1.** Peak strain linear regression data.

| Group | Intercept | Slope | $R^2$ |
|---|---|---|---|
| BL | -25.61 | 3945.53* | 0.818 |
| HU-7 | -103.121 | 3547.43* | 0.818 |
| HU-21 | -67.28 | 2876.00* | 0.662 |

*denotes P<0.001 for each correlation

Since the muscle contractions of this countermeasure were dosed to 120% of peak isometric torque, peak strain was also plotted versus torque expressed as a percent of peak isometric torque (Figure 17).

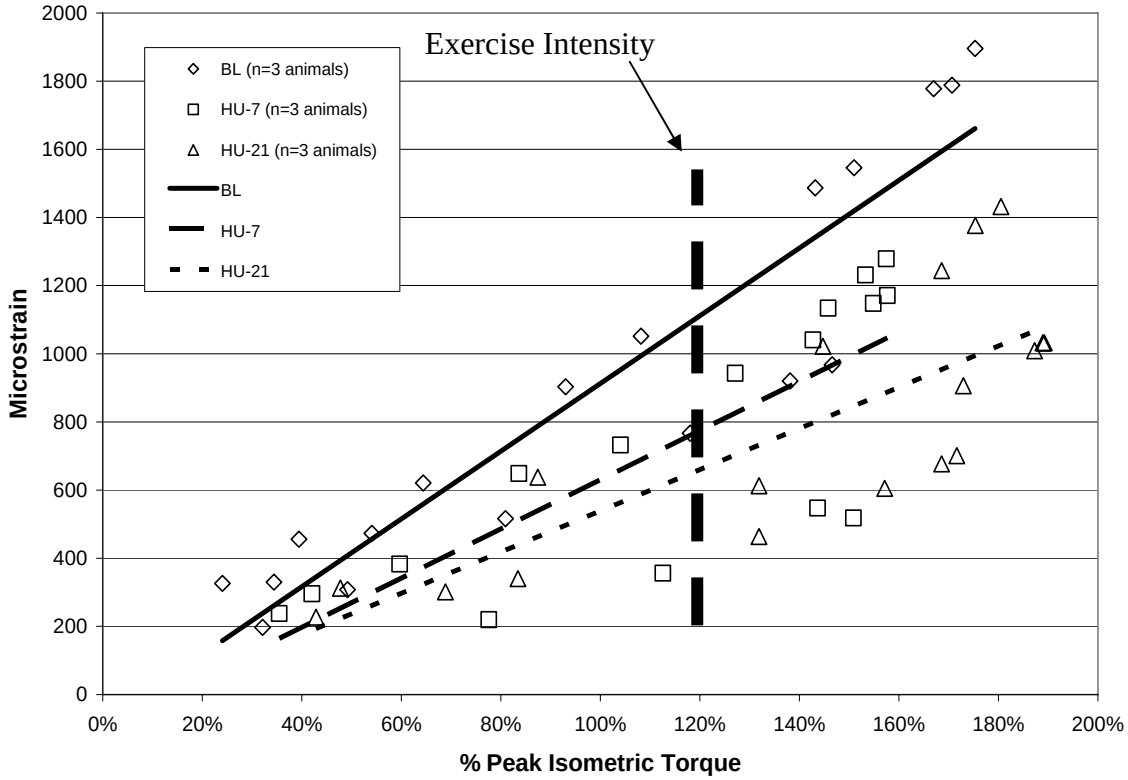


**Figure 17.** The peak strain vs. % peak isometric torque plot shows a larger decrease in peak strain at a given torque over time than when plotted against eccentric torque as well as decrease in slope.

The peak strain level at 120% of peak isometric torque decreased in the first 7 days from 1100 to 775 μstrain and from 775 to 660 μstrain after 7 days. There are no significant differences among groups for the slopes and intercepts when plotted against % peak isometric torque.

## 4.2 Average Strain

Average strain was plotted against eccentric torque for each group of animals and the resulting graph is shown in Figure 18.

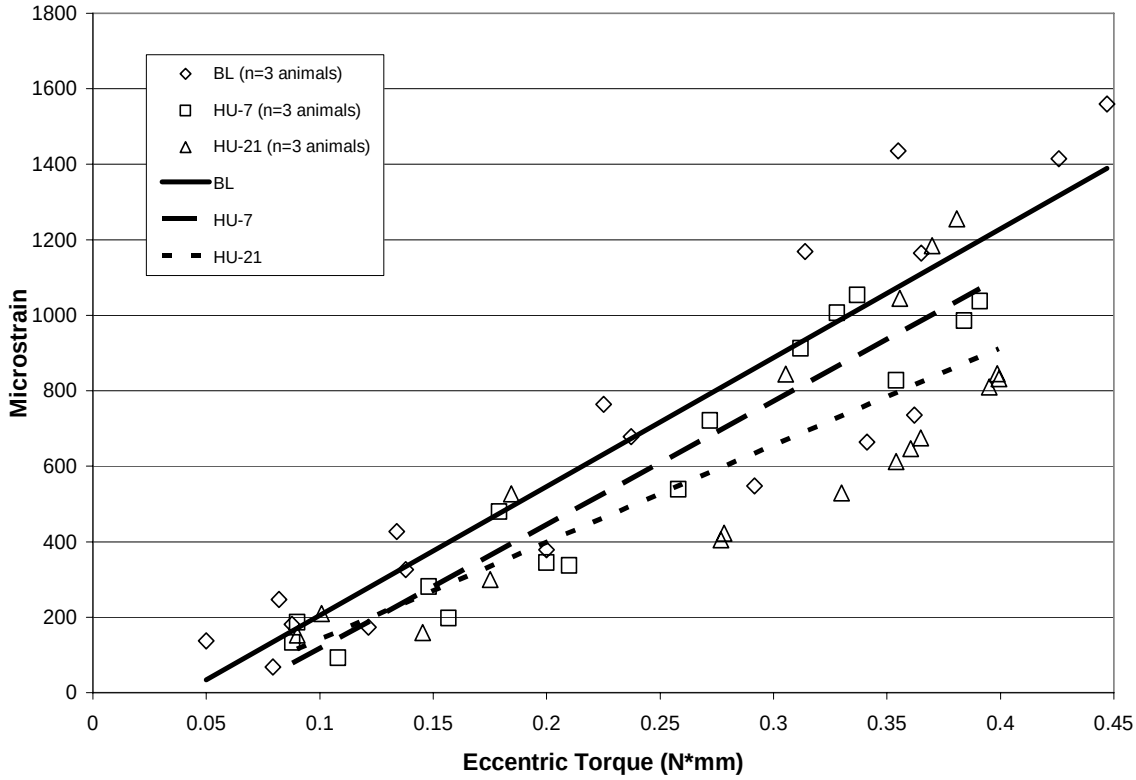


**Figure 18.** The average strain vs. eccentric torque plot demonstrates a decrease in average strain at a given torque over time. The slopes for BL and HU-7 are similar while the slope for HU-21 is lower.

The BL and HU-7 slopes are similar and the slope for the HU-21 group is lower than the other two. The intercepts for all three groups are near the same. The regression data are listed in Table 2 for each group of animals.

**Table 2.** Average strain linear regression data.

| Group | Intercept | Slope | $R^2$ |
|---|---|---|---|
| BL | -136.93 | 3415.20* | 0.831 |
| HU-7 | -210.64ψ | 3276.77* | 0.920 |
| HU-21 | -115.84 | 2571.68* | 0.671 |

ψ denotes P<0.05, * denotes P<0.001 for each correlation

While the curves shift downward for the HU-7 and HU-21 groups, there are no significant differences among the slopes and intercepts for the 3 groups.

The average strain was also plotted versus percent of peak isometric torque because the muscle stimulation intensity is based on percent of peak isometric torque (Figure 19).

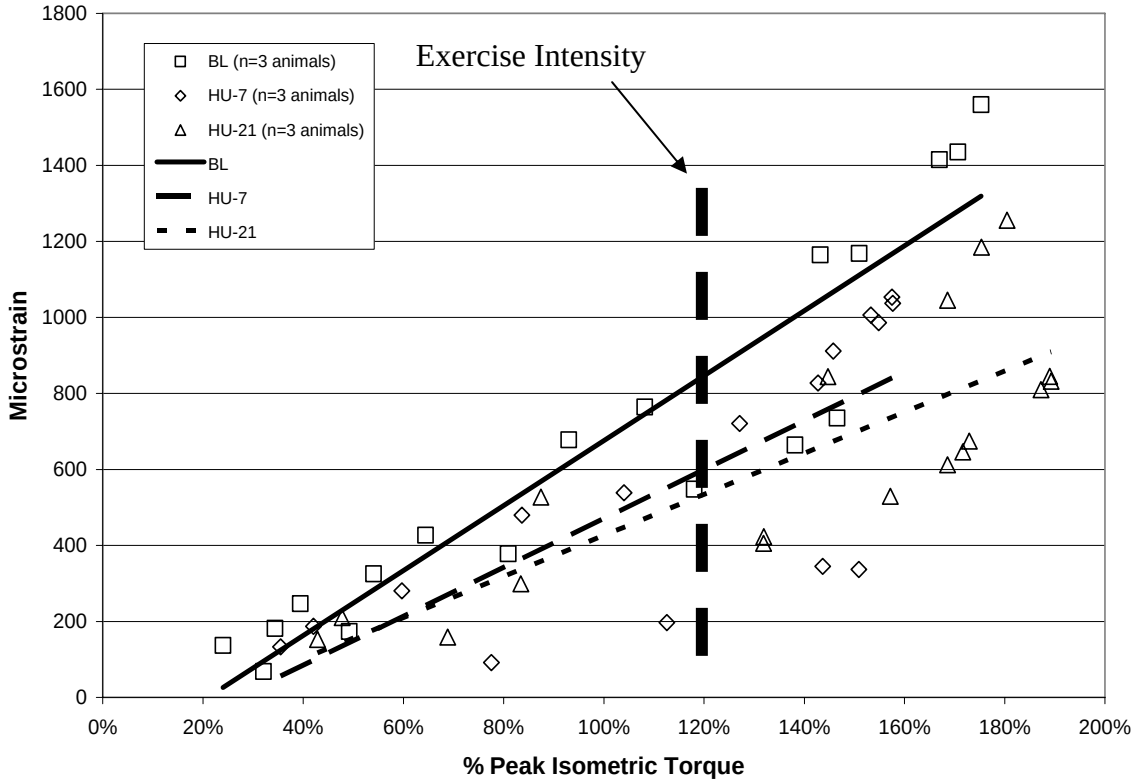


**Figure 19.** The average strain vs. % peak isometric torque plot shows a larger decrease in average strain at a given torque over time than with eccentric torque.

After the first 7 days, the average strain at 120% peak isometric torque decreased from 850 to 600 μstrain. Between Day 7 and Day 21, the average strain decreased to 530 μstrain. While there are no significant differences among the slopes and intercepts for the 3 groups, the strain at a given torque appears to decrease over the course of the study.

4.3 Initial Strain Rate

Initial strain rate was determined by calculating the average slope from the beginning of the stimulation to 0.1 seconds. These values were plotted against eccentric torque and are shown in Figure 20.

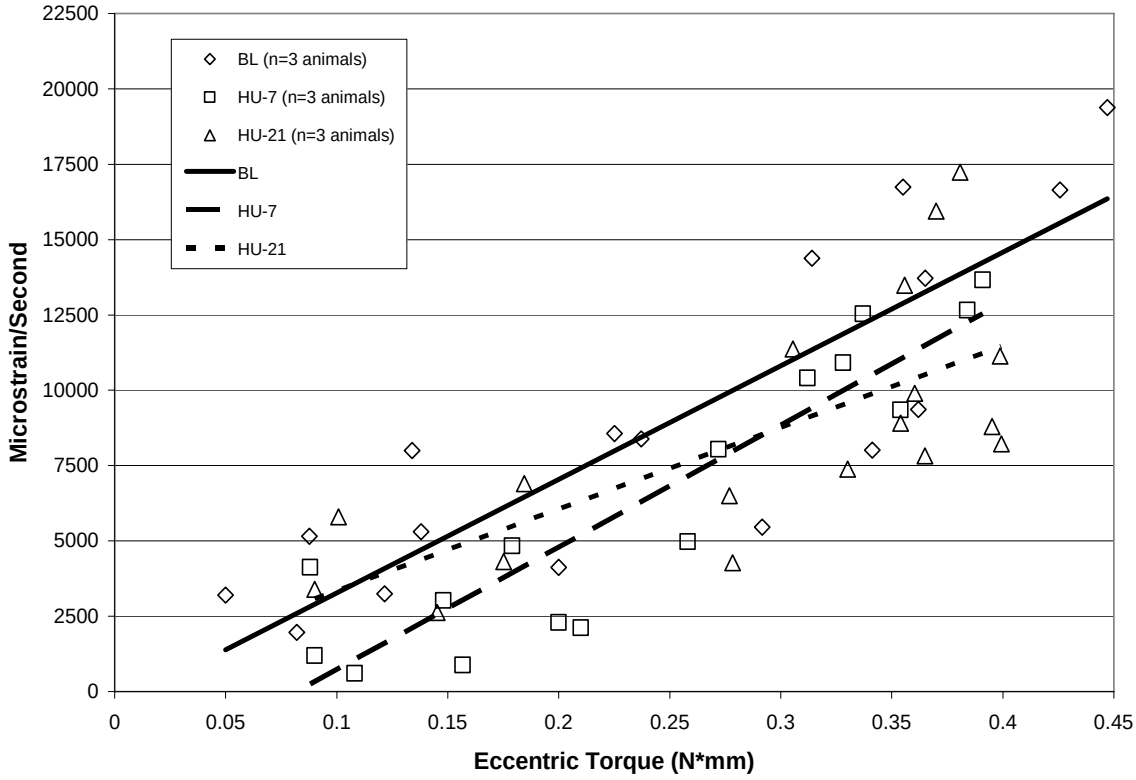


**Figure 20.** The initial strain rate vs. eccentric torque plot shows an initial decrease in the strain rate at a given torque by HU-7 and an increase between HU-7 and HU-21.

While slopes of the initial strain rate curves for the BL and HU-7 groups are very similar, the slope for the HU-21 group is much lower than for the BL and HU-7 groups and the intercepts are different among all groups (Table 3). The slopes and intercepts are not significantly different between groups even though the curves appear to decrease over time.

**Table 3.** Initial strain rate linear regression data.

| Group | Intercept | Slope | $R^2$ |
|---|---|---|---|
| BL | -497.10 | 37688.03* | 0.756 |
| HU-7 | -3328.50ψ | 40589.15* | 0.836 |
| HU-21 | 643.79 | 27047.25* | 0.491 |

ψ denotes P<0.05, * denotes P<0.001 for each correlation

The initial strain rates for each group were also plotted against percent of peak isometric torque in Figure 21.

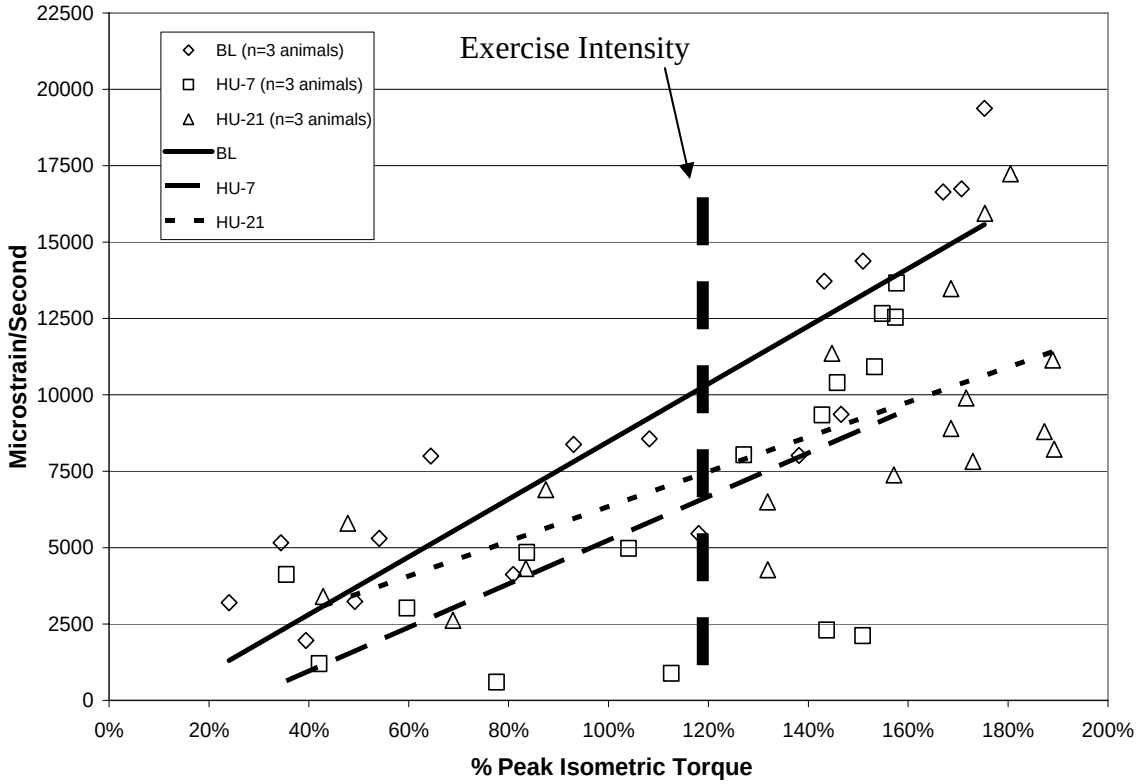


**Figure 21.** The initial strain rate vs. % peak isometric torque plot show a larger change in the strain rate at a given torque than when the strain rate is plotted against eccentric torque.

The initial strain rate at 120% peak isometric torque decreased from 10355 to 6670 μstrain/second between Days 0 and 7. The strain rate increased to 7500 μstrain/second at Day 21. There are no statistical differences among groups for the correlation coefficients.

## 4.4 Secondary Strain Rate

The secondary strain rate for each contraction was calculated by averaging the instantaneous strain rates between 0.1 and 0.4 seconds into the contraction. By averaging the instantaneous strain rates, small muscle twitches were eliminated, and the underlying rate was characterized. The secondary strain rates were then plotted against eccentric torque as shown in Figure 22.

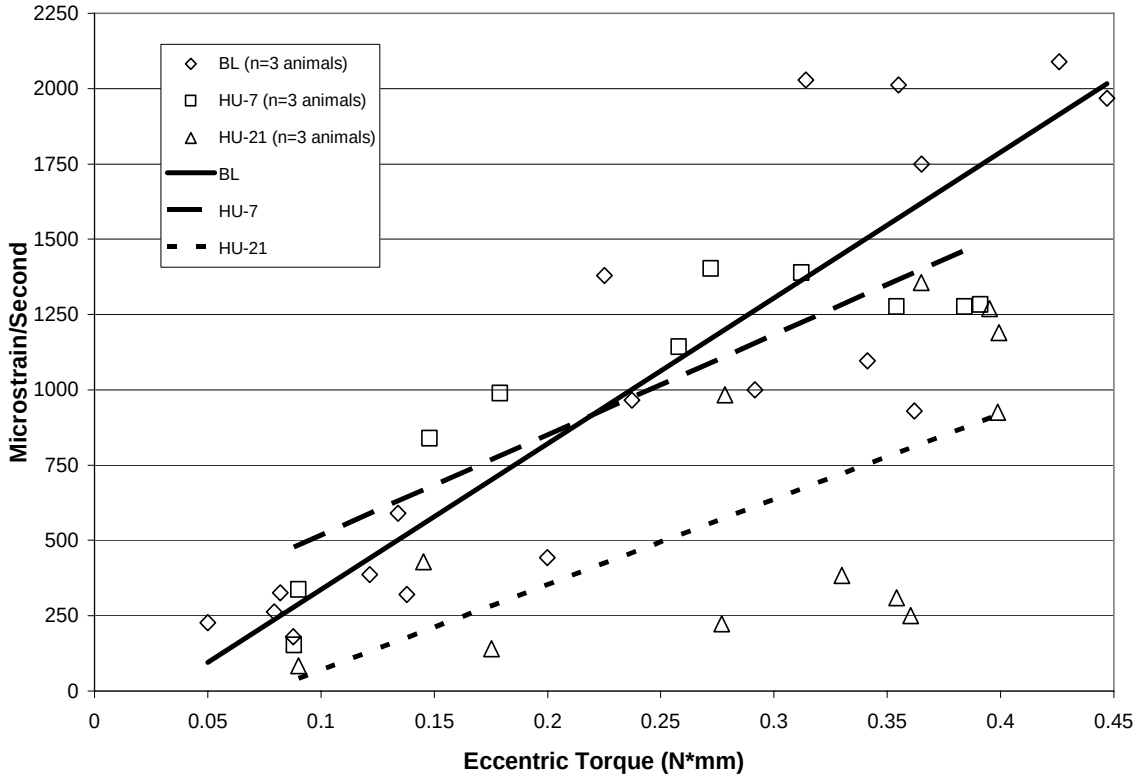


**Figure 22.** The secondary strain rate vs. eccentric torque graph shows differences between all three groups, but the slopes of the regression lines for HU-7 and HU-21 are similar.

The slopes for the HU-7 and HU-21 groups, which are similar, trend lower than the curve for the BL group (Table 4). The slopes for the 3 groups appear different; however, there are no statistically significant differences among the curves for the 3 groups.

**Table 4.** Secondary strain rate linear regression data.

| Group | Intercept | Slope | $R^2$ |
|---|---|---|---|
| BL | -147.40 | 4841.05* | 0.790 |
| HU-7 | 228.47 | 2842.18ψ | 0.455 |
| HU-21 | -191.37 | 3078.53* | 0.488 |

ψ Denotes P<0.005, * denotes P<0.001 for each correlation

Secondary strain rate was also plotted against percent of peak isometric torque in Figure 23.

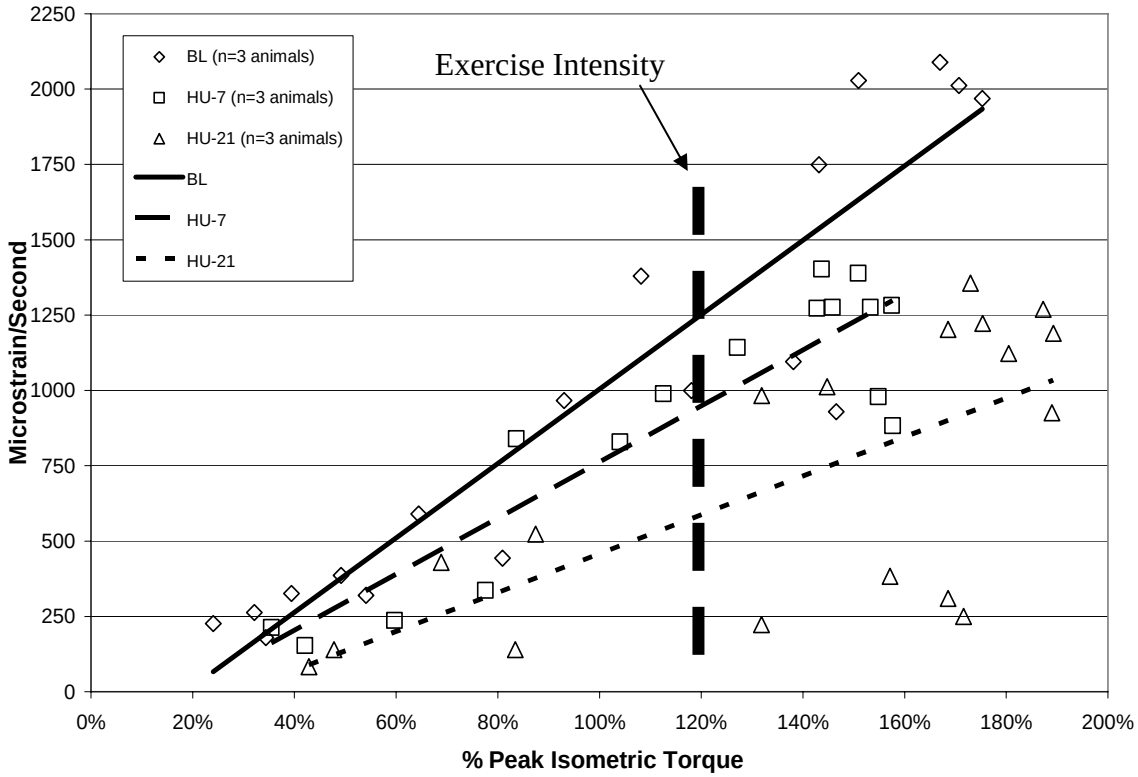


**Figure 23.** In the secondary strain rate vs. % peak isometric torque plot, there is a decrease in the slopes over time.

Secondary strain rate at 120% peak isometric torque decreased from 1250 to 950 μstrain/second between Day 0 and Day 7, while the rate decreased to 590 μstrain/second at Day 21. However, there are no significant differences between the slopes and intercepts for secondary strain rate versus torque.

## 4.5 Strain Mathematical Models

Although there are trends suggesting possible differences in the characteristics examined over time, the study was not designed to detect statistically significant differences among groups. Results for all 3 groups were therefore pooled to assess more broad and general relationships. In order to develop a mathematical model for each strain parameter, each parameter was plotted against eccentric torque for the animals in all groups. The data were also plotted as the log of the parameter versus eccentric torque. The semi-log method of plotting the data was used because the data for some parameters were not well suited for a purely linear relationship. Linear regression analysis was then performed for each parameter to determine the relationship.

### *4.5.1 Peak Strain Model*

Peak strain data for the animals in all three groups were plotted against eccentric torque in Figure 24. The $R^2$ value for the regression is 0.704 with a statistical power of 1. The intercept and slope for the regression line are -31.15 ($P>0.05$) and 3281.78 ($P<0.001$), respectively. Since $P>0.05$ for the intercept, the intercept is not significantly different from zero.

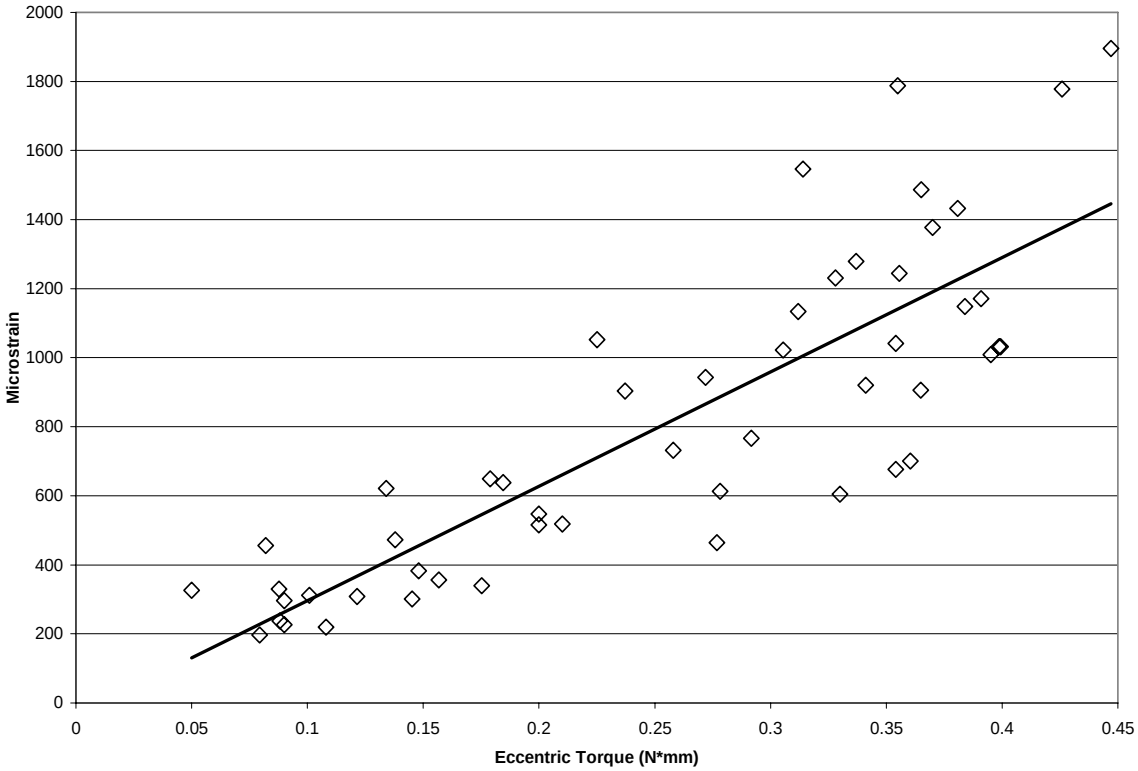


**Figure 24.** The peak strain vs. eccentric torque plot for animals in all three groups. The $R^2$ value for the regression line is 0.704.

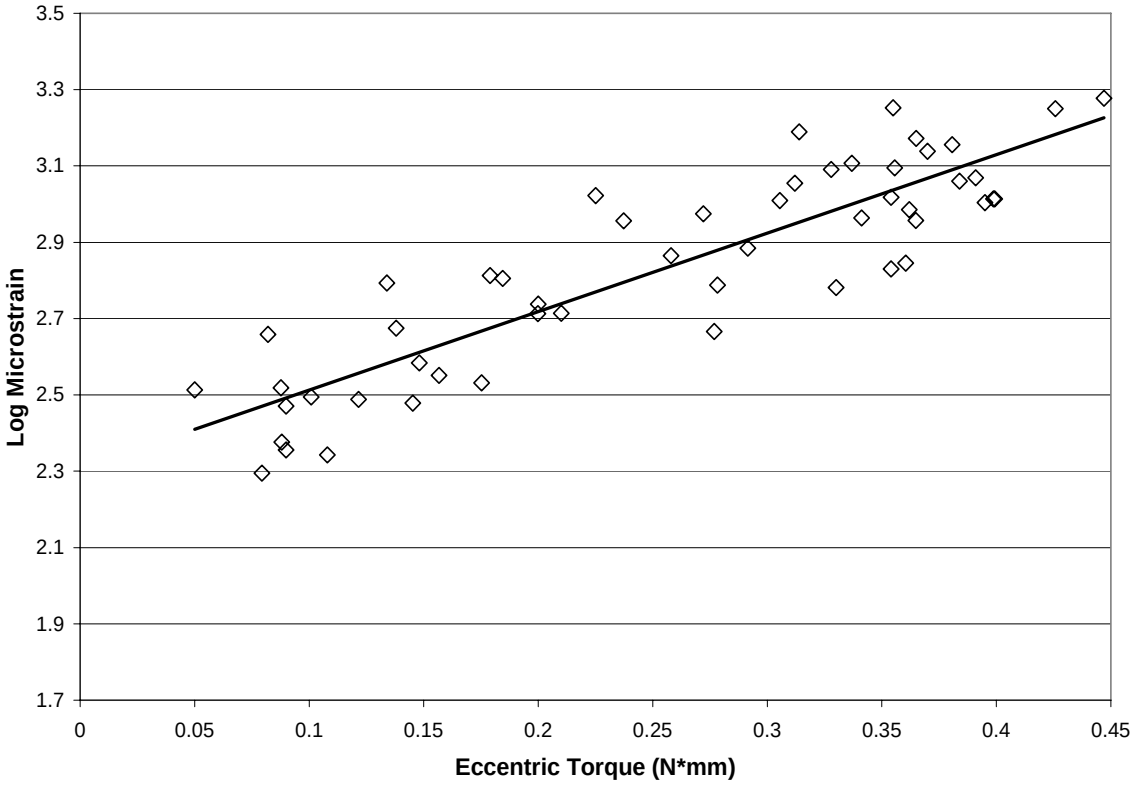


**Figure 25.** The log of peak strain vs. eccentric torque plot for animals in all three groups. The $R^2$ value for the regression line is 0.785.

The same data were also plotted as the log of peak strain versus eccentric torque as shown in Figure 25. The log plot for peak strain is a better fit for the data collected. The slope of the line is 2.057 ($P<0.001$) and the intercept is 2.307 ($P<0.001$). The $R^2$ value for the linear regression is 0.785 with a statistical power of 1. Based on the $R^2$ values, the log peak strain vs. eccentric torque is a better fit and is thus the preferred mathematical model. The best fit relationship for the peak strain is

$$\mu strain = 10^{(2.057*T+2.307)}, \qquad \text{(Equation 3)}$$

where T is peak eccentric torque (N*mm).

### *4.5.2 Average Strain Model*

Average strains for all three time points were plotted against eccentric torque as shown in Figure 26.

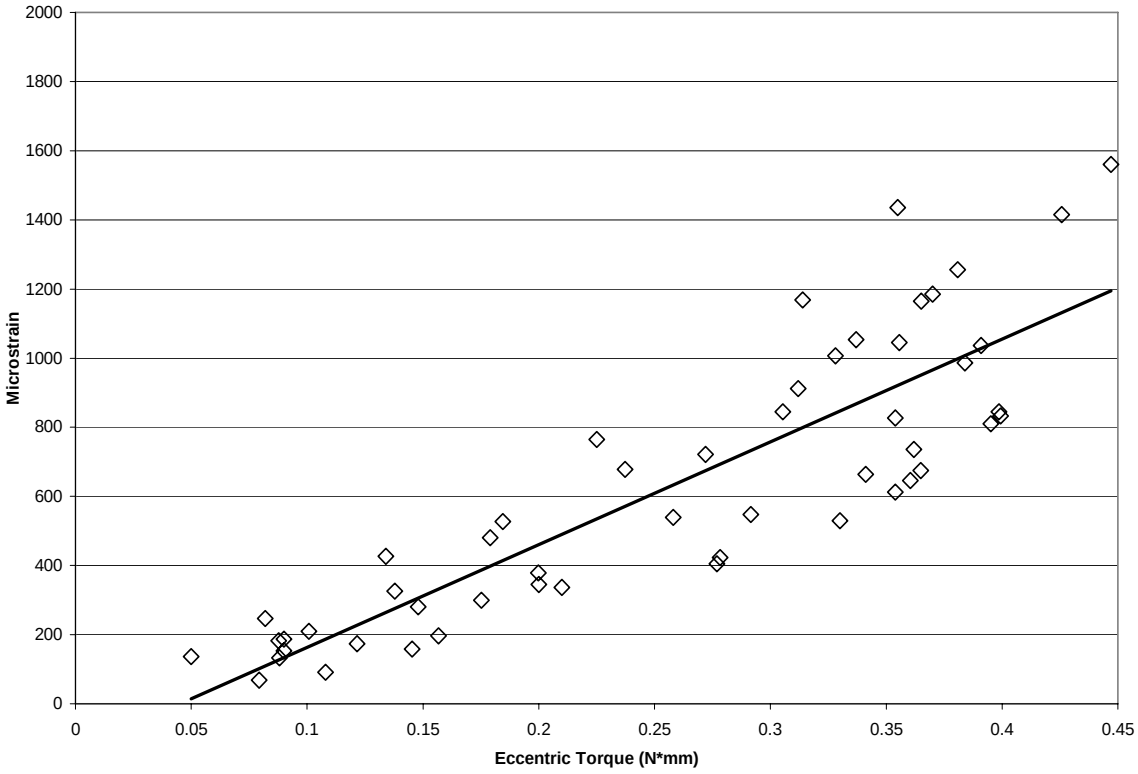


**Figure 26.** The average strain vs. eccentric torque plot for the animals in all three groups. The $R^2$ value for the regression line is 0.757.

The $R^2$ value for the above regression is 0.757 with a statistical power of 1. The intercept for the regression line is -134.57 ($P<0.05$) and the slope is 2973.43 ($P<0.001$). The log of average strain was plotted against eccentric torque and is shown in Figure 27.

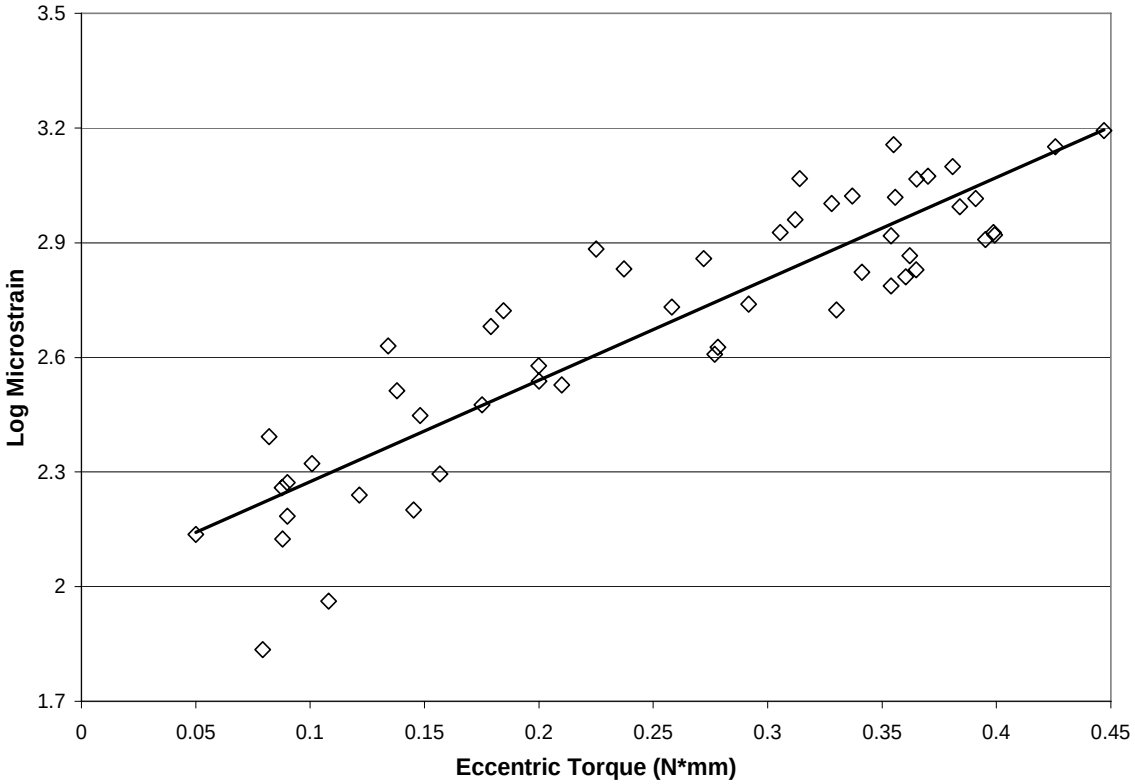


**Figure 27.** The log of average strain vs. eccentric torque for the animals in all three groups. The $R^2$ value for the regression line is 0.816.

The regression line for the log of average strain is a better fit than the previous model with $R^2$=0.816 and a statistical power of 1. The slope is 2.653 (P<0.001) and the intercept is 2.009 (P<0.001). Since the regression equation for the log average strain vs. eccentric torque has a higher $R^2$ value, it is the preferred mathematical model for average strain. The model for average strain is

$$\mu strain = 10^{(2.653*T+2.009)}, \qquad \text{(Equation 4)}$$

where T is peak eccentric torque (N*mm).

### *4.5.3 Initial Strain Rate Model*

The initial strain rate for animals in all three groups was plotted versus eccentric torque in Figure 28.

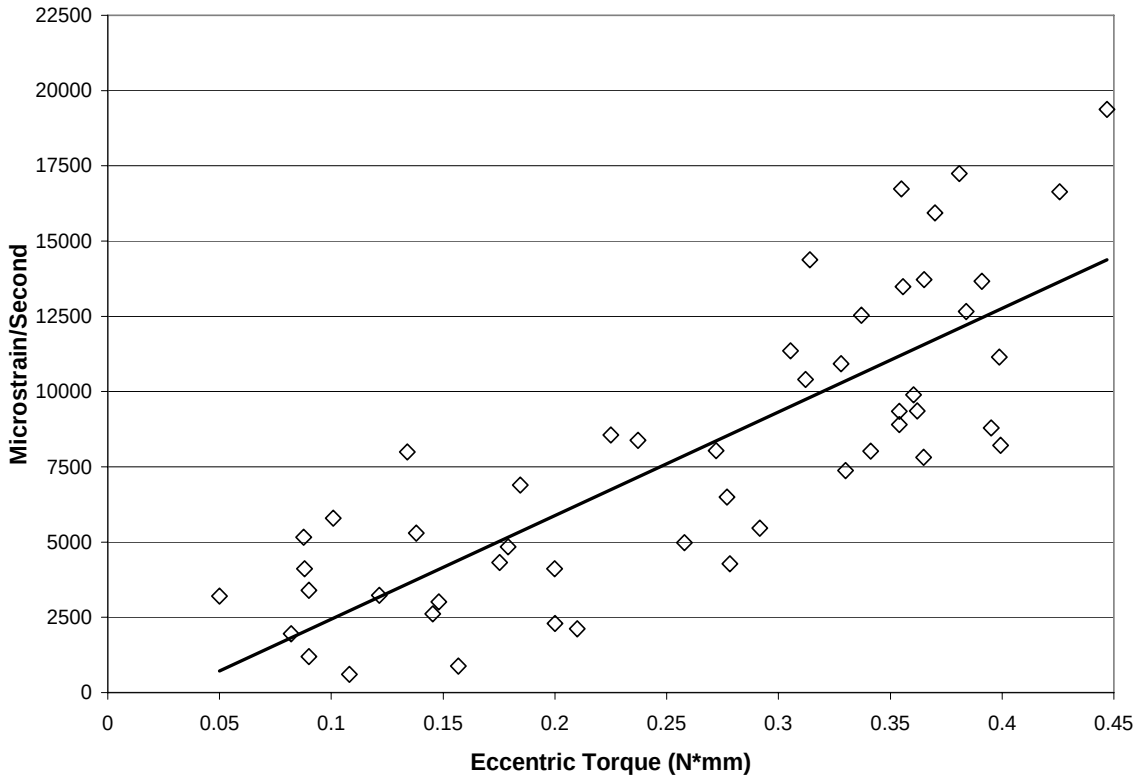


**Figure 28.** The initial strain rate vs. eccentric torque plot for the animals in all three groups. The $R^2$ value for the regression line is 0.671.

The $R^2$ value for the above regression is 0.671 with a statistical power of 1. The intercept of the line is -998.60 ($P>0.05$) and the slope is 34415.56 ($P<0.001$). For the intercept, $P>0.05$, so the intercept is not significantly different from zero. The log of initial strain rate was plotted against eccentric torque shown in Figure 29.

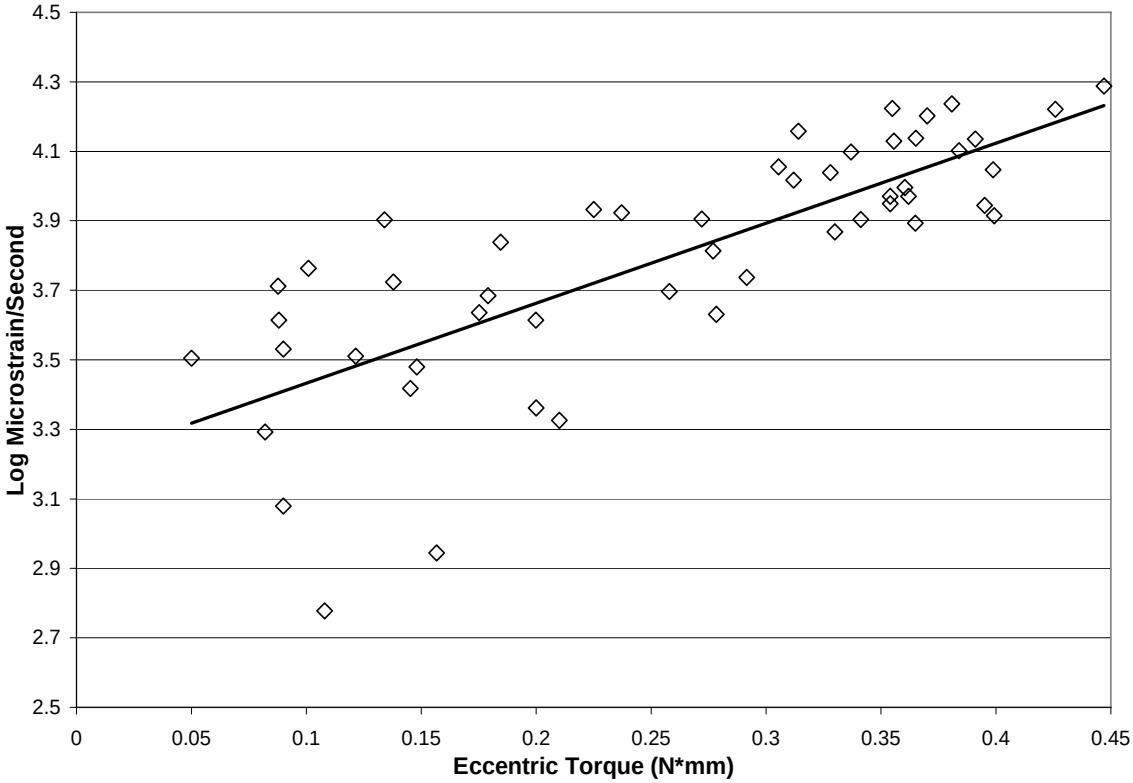


**Figure 29.** The log of initial strain rate vs. eccentric torque plot for the animals in all three groups. The $R^2$ value for the regression line is 0.605.

The intercept and slope of the regression line are 3.202 (P<0.001) and 2.306 (P<0.001) respectively with $R^2$=.605 and a statistical power of 1. The previous regression line is a better correlation than the plot of log initial strain rate because of the higher $R^2$ value, so the preferred model for initial strain rate is

$$\frac{\mu strain}{s} = 34415.56 * T, \qquad \text{(Equation 5)}$$

where T is peak eccentric torque (N*mm).

### *4.5.4 Secondary Strain Rate Model*

The secondary strain rate for the animals in all three groups was plotted versus eccentric torque as shown in Figure 30.

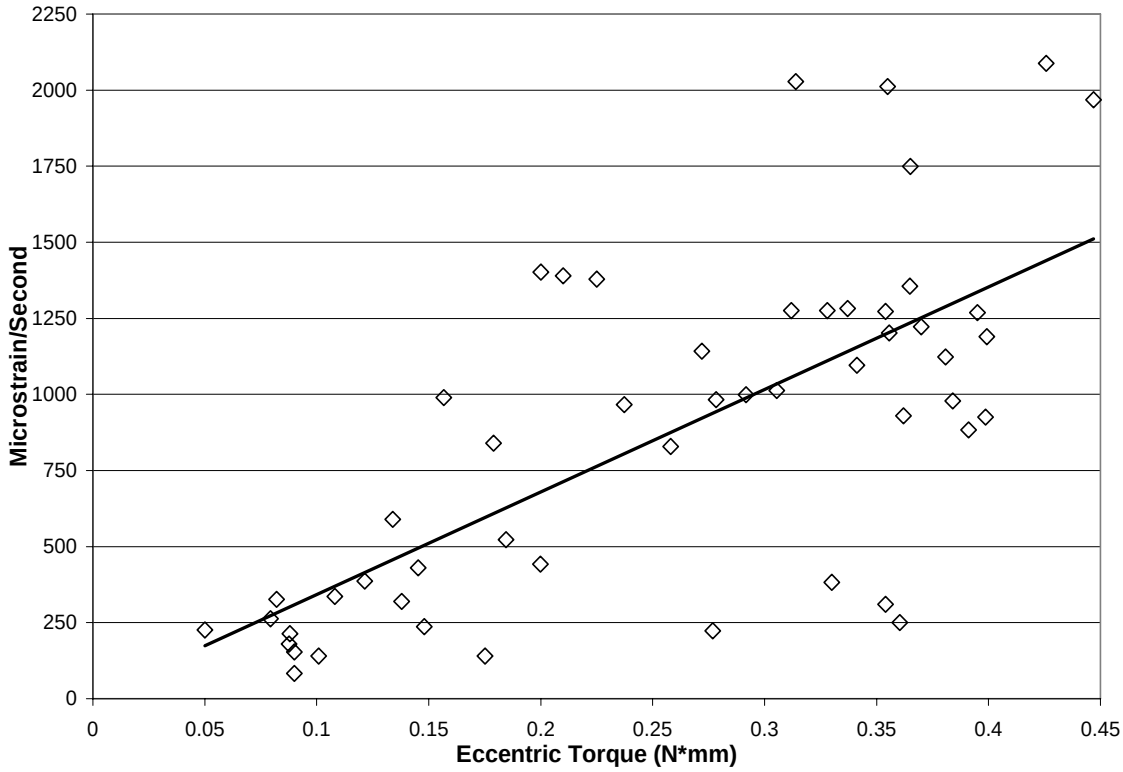


**Figure 30.** The secondary strain rate vs. eccentric torque plot for the animals in all three groups. The $R^2$ value for the regression line is 0.504.

The $R^2$ value for the above regression is 0.504 with a statistical power of 1. The intercept of the line is -19.50 ($P>0.05$) and the slope is 3414.41 ($P<0.001$). Since $P>0.05$ for the intercept, the intercept is not significantly different from zero. The log of secondary strain rate was also plotted versus eccentric torque in Figure 31.

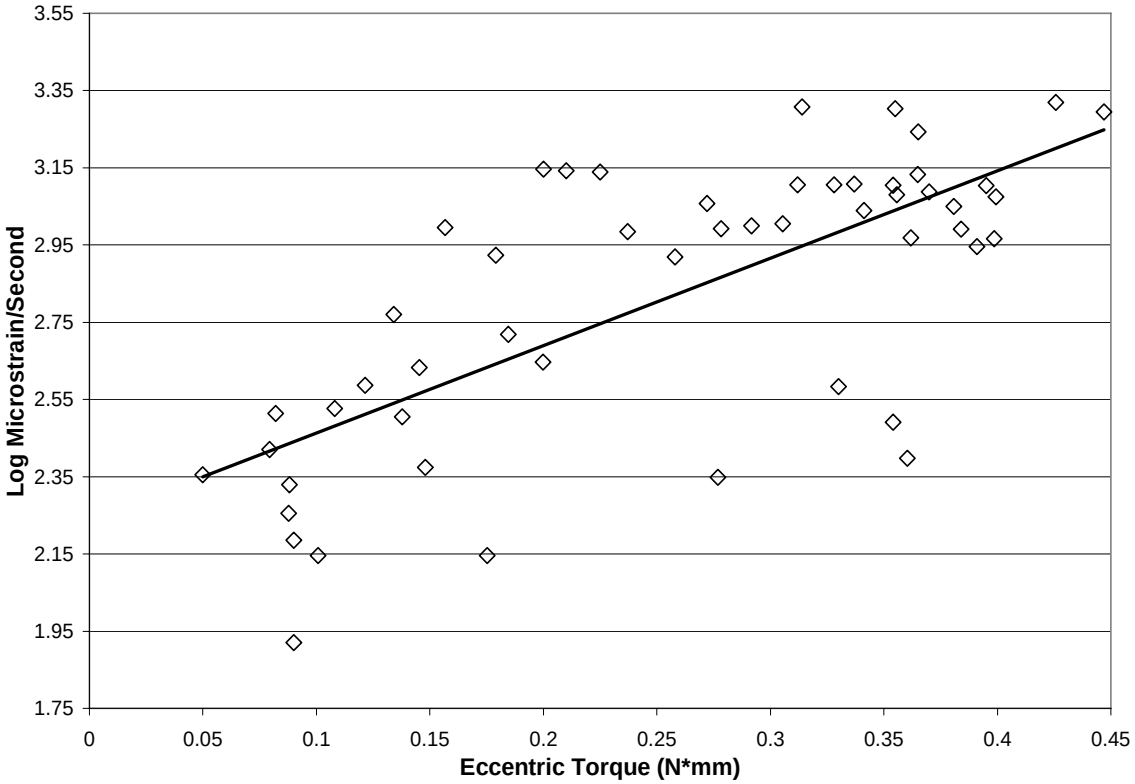


**Figure 31.** The log of secondary strain rate vs. eccentric torque plot for the animals in all three groups. The $R^2$ value for the regression line is 0.512.

The intercept and slope of the regression line are 2.236 (P<0.001) and 2.265 (P<0.001) respectively with $R^2$= 0.512 and a statistical power of 1. The log secondary strain rate vs. eccentric torque has a higher $R^2$ value; therefore the preferred model for secondary strain rate is

$$\frac{\mu strain}{s} = 10^{(2.265T*2.236)}, \qquad \text{(Equation 6)}$$

where T is peak eccentric torque (N*mm).

## 4.6 Mathematical Model versus Measured Values

The mathematical relationships between strain parameters and eccentric torque were compared to measured values to determine the accuracy of the model. The plot for peak strain and the mathematical model is shown in Figure 32.

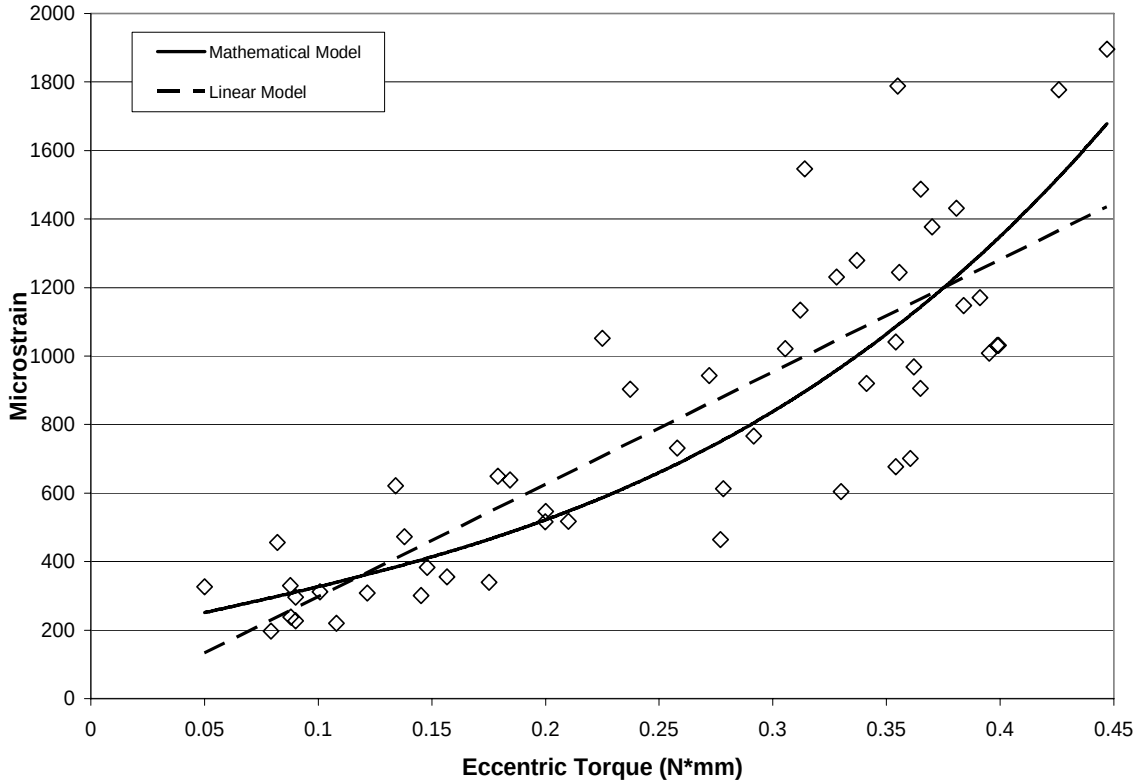


**Figure 32.** The mathematical model for peak strain shows an average difference of 4.0% from measured values.

The model predicts the peak strain for a given eccentric torque within an average difference of 4.0%. The plot for average strain and the mathematical model is shown in Figure 33.

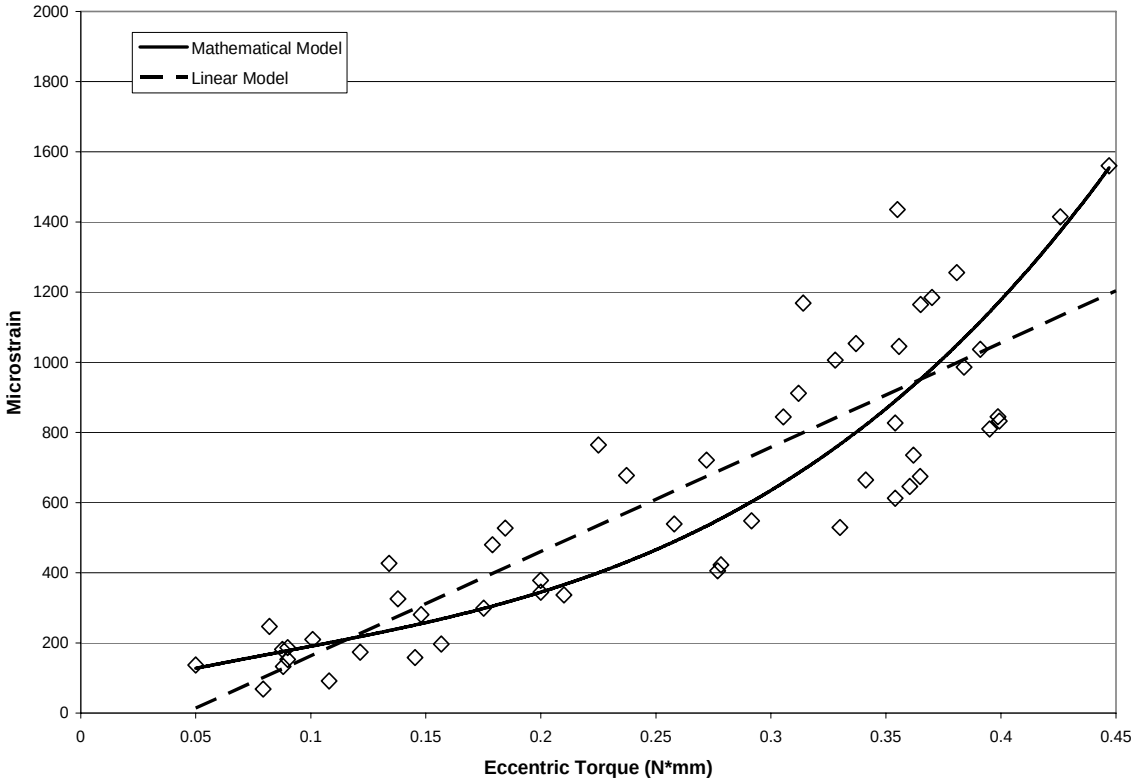


**Figure 33.** The mathematical model for average strain shows an average difference of 5.7% from measured values.

The model for average strain predicts the value within an average of 5.7% of the measured values. The plot for initial strain rate and the mathematical model is shown in Figure 34.

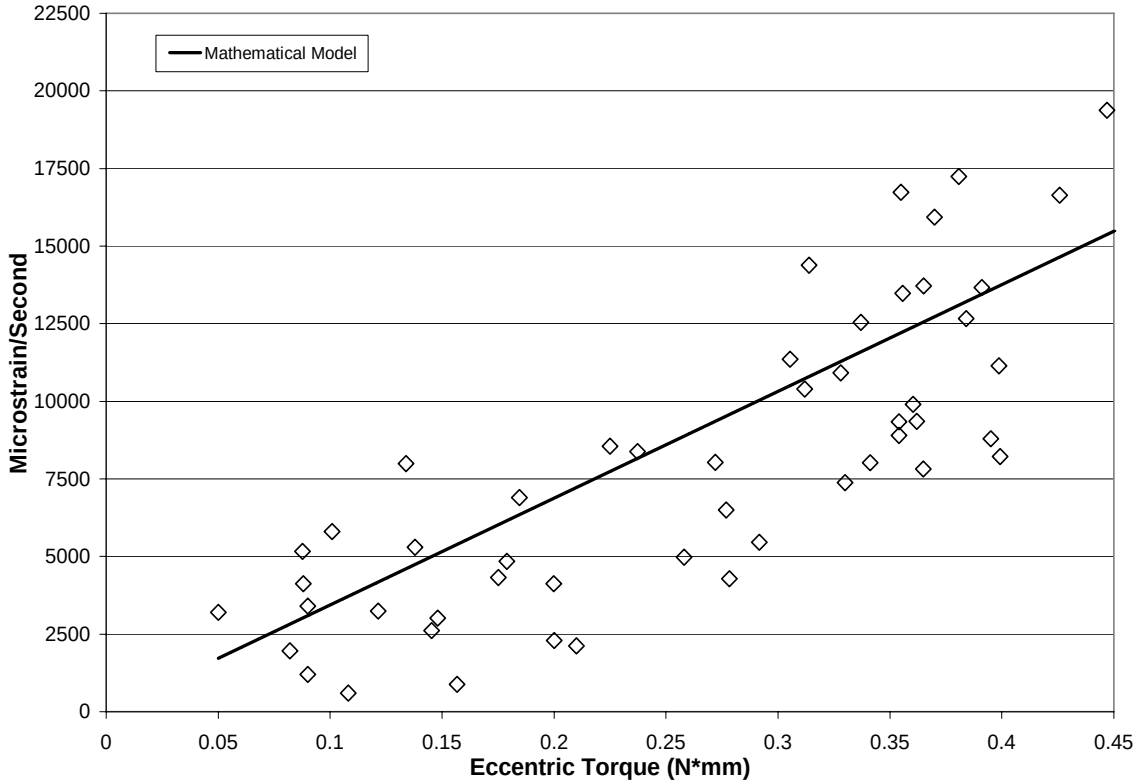


**Figure 34.** The mathematical model for initial strain rate shows an average difference of 11.2% from measured values.

The initial strain rate model predicts the value within 11.2% of measured values. The plot for secondary strain rate and the mathematical model is shown in Figure 35.

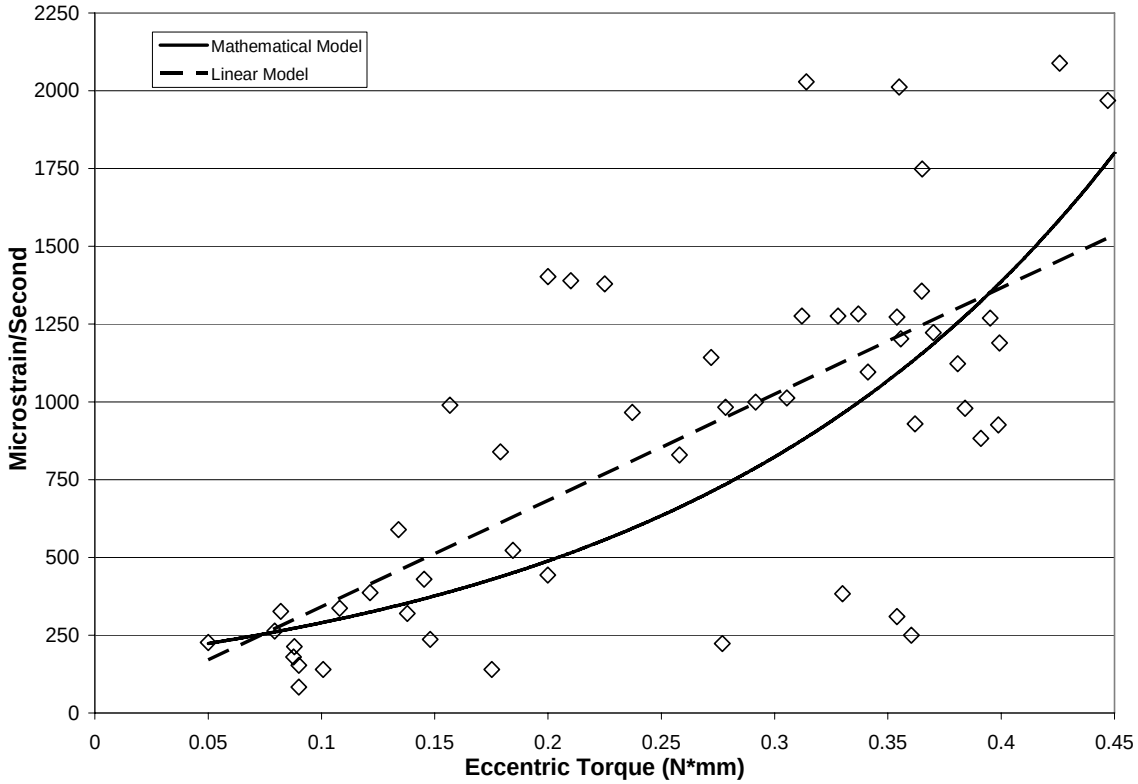


**Figure 35.** The mathematical model for secondary strain rate shows an average difference of 20.8% from measured values.

The secondary strain rate model predicts the values within 20.8% of measured values. The four models average less than 12.0% difference from measured values with the exception of the secondary strain rate which has a difference of 20.8%. The equations for each mathematical model are shown in Table 5, along with the average percent difference from measured values.

**Table 5.** Mathematical models and percent difference from measured values.

| **Strain Parameter** | **Mathematical Model** | **Average % Difference from Measured** |
|---|---|---|
| Peak Strain | $\mu strain = 10^{(2.057*T+2.307)}$ | 4.0 |
| Average Strain | $\mu strain = 10^{(2.653*T+2.009)}$ | 5.7 |
| Initial Strain Rate | $\frac{\mu strain}{s} = 34415.56*T$ | 11.2 |
| Secondary Strain Rate | $\frac{\mu strain}{s} = 10^{(2.265T*2.236)}$ | 20.8 |

# 5. DISCUSSION

## 5.1 Relevance to Previous Studies

The only other study to examine strain at the antero-medial aspect of the proximal diaphysis of the tibia during electrical muscle stimulation as a countermeasure to hindlimb unloading in rats is by Midura, et al. [21]. In the Midura study, a stimulation frequency of 30 Hz was administered through surface electrodes placed over the thigh above the knee [21]. The stimulation administered through the surface will not activate the plantarflexors the same as the percutaneous electrodes used in the current study. Peak strain measured by Midura, et al. was approximately 400 μstrain; however, there was a static strain component of 200 μstrain [21]. To trigger new bone formation, dynamic strain is necessary; therefore, the effective portion of strain in the Midura study was only 200 μstrain [21]. The peak strain measured in the current study at 30 Hz is consistent with the peak strain measured by Midura, et al. [21].

## 5.2 Osteogenic Potential

The peak strain at the antero-medial surface of the proximal diaphysis of the tibia during the exercise protocol was between 660 and 1,100 μstrain. The minimum peak strain magnitude for osteogenesis, which is an increase in new bone formation above normally observed levels, in normally ambulating rats is 1,000 μstrain at the midshaft of the tibia [9]. While the upper portion of the range of peak strains during electrical muscle stimulation are above 1,000 μstrain, most exercise sessions after the beginning of the study were below 1,000 μstrain. When only considering 1,000 μstrain as the strain threshold for osteogenesis, the electrical muscle stimulation exercise does not appear adequate to provide new bone formation. However, this threshold is applicable to bone formation in ambulating rats and this study looked at rats subjected to hindlimb unloading. In hindlimb unloaded rats, maintained bone structure as opposed to new bone formation is the desired outcome for a resistance exercise protocol. For bone homeostasis, the physiological strain window is around 200-1,500 μstrain [4]. Therefore,

the peak strains experienced during electrical muscle stimulation protocol would be expected to be high enough to maintain the structure of the bone.

Another issue is the location of the peak strain thresholds. The previously mentioned peak strain thresholds are all for locations at the mid-diaphysis of the tibia and strain in this study was measured at the antero-medial surface of the proximal diaphysis of the tibia. Osteogenic thresholds for peak strain decrease further toward the proximal end of the ulna [(7)]. The strain threshold may also decrease further away from the midshaft of the tibia. Considering the location of measured strain and the desired outcome of the electrical muscle stimulation protocol, the peak strain experienced is more than adequate to provide normal maintenance of the tibia and counteract bone loss due to hindlimb unloading. The strain thresholds from previous studies apply to cortical bone at the mid-diaphysis, but for adult hindlimb unloaded rats bone loss is most prominent in the cancellous compartment at the proximal metaphysis of the tibia [(17)]. Therefore, it is not clear whether the measured strain levels will prove to be osteogenic or not for cancellous bone in the proximal metaphysis of the tibia.

Average strain during the muscle stimulation protocol was also examined. The average strain at the antero-medial surface of the proximal diaphysis of the tibia during the exercise protocol was between 530 and 850 μstrain. The effect of average strain on osteogenesis has not been examined; however, the average strains during electrical muscle stimulation fall within the physiological window. Along with the peak strains the average strains during the protocol are enough to lead to normal bone maintenance and possibly new bone formation. While the average strain has not been shown to have an effect on bone formation, the average strain was included in this study to further characterize the strain profile during electrical muscle stimulation.

Strain rate is also an important factor in triggering bone remodeling. The initial strain rate during muscle contractions is of particular interest due to higher values than the secondary strain rate. The initial rate has more effect on osteogenesis because it generates higher fluid shear stresses in the bone. The initial strain rate for eccentric muscle contractions at the antero-medial surface of the proximal diaphysis of the tibia

during the exercise protocol was between 6,670 and 10,350 μstrain/second. A strain rate of 4,800 μstrain/second is known to produce a bone response at the mid-diaphysis of the tibia [9]. The strain rates observed in this study are considerably higher than 4,800 μstrain/second and are believed to be enough to obtain a bone response in the proximal tibia. The secondary strain rate at the antero-medial surface of the proximal diaphysis of the tibia during the exercise protocol was between 590 and 1,250 μstrain. These levels are not high enough to generate a bone response [9]. The initial strain rate is more important for osteogenesis than secondary strain due to the higher magnitudes of the initial strain rate; however, secondary strain was included in the study to more fully characterize the shape of the strain profile during electrical muscle stimulation.

As stated previously, number of daily cycles as well as rest inserted in between loading cycles affects osteogenic potential. For the levels of peak strain and initial strain rate experienced during the electrical muscle stimulation protocol, 36 or more cycles per day for three days a week are required for bone formation [9]. The muscle stimulation protocol in this study consists of 40 cycles per day for three days a week and is enough to produce new bone formation. A ten second rest period is inserted between each contraction as well as a two minute rest between each 10 contraction set. These rest periods allow the extracellular fluid in the bone to return to its resting state. The rest periods also allow the muscles to recover in order to maintain a higher level of force applied by the muscles. Given an optimum number of daily cycles and inserted rest periods, the eccentric contractions experienced during electrical muscle stimulation will produce bone formation in the tibia.

### 5.3 Change in Strain over Time

The strain parameters observed after 7 days of hindlimb unloading with electrical muscle stimulation as compared to those observed in baseline control rats at day 0 have similar slopes but the curve is shifted lower for the 7 day group. While this decrease is not statistically significant, there is a trend over time. The decrease in strain from the baseline group to the 7 day group is possibly caused by a shift in loading of the tibia

caused by atrophy of skeletal muscles due to hindlimb unloading [24]. This shift in loading of the tibia may contribute to the decrease in both peak and average strain. The atrophy in the plantarflexors may also be responsible for the decreases in strain rate after 7 days.

The slope for strain parameters, other than secondary strain rate, decreased between the 7 day group and 21 day groups. The changes in the slope of the curves for rats hindlimb unloaded for 21 days and exercised 3 days per week are possibly caused by increased cross-sectional geometry of the tibia. An increase in cross-sectional area would lead to lower strain levels with equal applied loads due to the increased stiffness of the bone. As stated previously, the exercise countermeasure creates loading that exceeds osteogenic strain thresholds for bone formation. The increased bone formation from applied loading may lead to an increase in bone stiffness over time and as a consequence could lower strain experienced in the tibia. The first bone to change due either loading or unloading is trabecular bone. If new trabecular bone is added as a result of the exercise countermeasure, the overall stiffness of the bone would increase. An increase in stiffness will cause a decrease in strain given the same force, because the bone resists deformation.

## 5.4 Mathematical Model of Strain

An important objective of this study was to obtain mathematical models to relate different strain parameters to eccentric torque. These relationships will be used in future studies examining the effects of electrical muscle stimulation as a countermeasure for hindlimb unloading. The relationships will allow for the estimation of strain in the tibia during exercise without requiring the use of strain gages attached to the bone surface. There is less than 7% difference between the mathematical models for peak strain, average strain and secondary strain rate and the actual results for each parameter. For initial strain rate, there is less than a 12% difference between the model and the actual results. The differences between the models and actual results for the strain parameters are within an acceptable range for biological systems. The model for secondary strain

rate is more than 20% different from measured values, and therefore would not predict the secondary strain rate accurately. With the exception of secondary strain rate model, the mathematical relationships developed in this study are excellent models for determining the strain characteristics during the electrical muscle stimulation countermeasure for hindlimb unloading in rats.

# 6. CONCLUSION AND RECOMMENDATIONS

## 6.1 Conclusion

This study examined strain in the proximal tibia of rats during electrical muscle stimulation. The strains measured during the muscle stimulation protocol provide valuable insight into mechanical loads on bone generated during the muscle contraction. By characterizing the strain on the surface of the tibia at different time points during hindlimb unloading, changes in bone loading patterns during electrical muscle stimulation were observed that may provide insight into bone changes during hindlimb unloading coupled with the muscle stimulation countermeasure. The decreasing trend in strain parameters observed during the course of the study suggests a decrease in the muscle's ability to generate torque at the ankle as well as an increase in stiffness of the tibia. Based on the strain parameters measured during the course of this study, the stimulated eccentric contraction countermeasure would be expected to effectively counteract bone loss due to hindlimb unloading.

An important objective of this study was to create a mathematical model to relate strain parameters to peak ankle torque during electrical muscle stimulation. This model will facilitate the estimation of strains during muscle stimulation without the need to apply a strain gage to the bone surface. In subsequent studies of the effectiveness of the electrical muscle stimulation countermeasure for bone loss due to microgravity, records of strain in the tibia can be collected throughout the 28 day study. The mathematical model generated during the study predicts strain in the proximal tibia within 12% of the actual value based on the eccentric torque measured at the ankle during muscle stimulation.

## 6.2 Recommendations

Implanting a tri-axial (rosette) strain gage on the antero-medial surface of the proximal diaphysis of the tibia would provide more detailed characterization of strain during the electrical muscle stimulation exercise protocol. Rosette strain gages measure

strain in three directions and these strains used to calculate principal strains on the bone surface. Determining the principle strains on the surface allows for differentiation of normal and shear strains as well as principle strain magnitude and direction. These strain components may provide more insight into the osteogenic potential of the electrical muscle stimulation protocol. A complication which arises when implanting rosette strain gages is the increased size over uni-axial gages. There is very little area anywhere on the tibia to attach a rosette strain gage. The antero-medial surface of the proximal diaphysis is the largest surface on the tibia which makes it the best location to attach a rosette strain gage.

A better understanding of loads imposed on the tibia during hindlimb unloading would lead to a better understanding of strain levels required to prevent bone loss during unloading. While the effects of hindlimb unloading on bone remodeling are known, muscle loading applied to bone is not as well documented. Implanting a strain gage in a hindlimb unloaded rat without any intervention would give insight into strain levels experienced during unloading. Along with strain during hindlimb unloading, characterizing strain during normal ambulation would provide useful information for determining the osteogenic potential of electrical muscle stimulation. For measuring strain during both hindlimb unloading and ambulation, a method for attaching a strain gage to the bone surface for longer periods of time is necessary. With the adhesive used for strain gage attachment in this study, the gage remains affixed to the bone surface for approximately 30 minutes. This time period is not long enough for strain measurement during periods of hindlimb unloading or normal ambulation. A possible alternative for strain adhesion is a different type of cyanoacrylate which is marketed as Dermabond (Ethicon Inc., Cornelia, GA). This adhesive has the potential to affix a strain gage to the bone surface for several days before the adhesive degrades. Closing the incisions is another issue when measuring strain in animals which cannot be anesthetized during measurements.

# REFERENCES


1. Ruff C, Holt B, Trinkaus E 2006 Who's afraid of the big bad Wolff?: "Wolff's Law" and bone functional adaptation. *Am J Phys Anthropol* **129**(4):484-498.
2. Baron R. 2003. General Principles of Bone Biology. *Primer on the Metabolic Bone Diseases and Disorders of Mineral Metabolism*. 5th ed. ASBMR. Washington, DC, USA, 1-8.
3. Alberts B, Bray D, Lewis J, Raff M, Roberts K, Watson JD 1994 *Molecular Biology of the Cell*, 3rd ed. Gerland Publishing, Inc. New York, NY, USA, 1185-1186.
4. Turner CH 1999 Toward a mathematical description of bone biology: the principle of cellular accommodation. *Calcif Tissue Int* **65**:466-471.
5. Hsieh Y, Turner C 2001 Effects of loading frequency on mechanically induced bone formation. *J Bone Miner Res* **16**:918-924.
6. Hsieh YF, Wang T, Turner CH 1999 Viscoelastic response of the rat loading model: implications for studies of strain-adaptive bone formation. *Bone* **25**:379-382.
7. Hsieh YF, Robling AG, Ambrosius WT, Burr DB, Turner CH 2001 Mechanical loading of Diaphyseal bone in vivo: the strain threshold for an osteogenic response varies with location. *J Bone Miner Res* **16**:2291-2297.
8. De Souza RL, Matsuura M, Eckstein F, Rawlinson SCF, Lanyon LE, Pitsillides AA 2005 Non-invasive axial loading of mouse tibiae increases cortical bone formation and modifies trabecular organization: a new model to study cortical and cancellous compartments in a single loaded element. *Bone* **37**(6):810-818.
9. Cullen D, Smith R, Akhter MP 2001 Bone-loading response varies with strain magnitude and cycle number. *J Appl Physiol* **91**:1971-1976.
10. Rabkin BA, Szivek JA, Schonfeld JE, Halloran BP 2001 Long-term measurement of bone strain in vivo: the rat tibia. *J Biomed Mater Res* **58**:277-281.

11. Burr DB, Milgrom C, Fyhrie D, Forwood M, Nyska M, Finestone A, Hoshaw S, Salag E, Simkin A 1996 In vivo measurement of human tibial strains during vigorous activity. *Bone* **18**:405-410.
12. Srinivasan S, Weimer D, Agans S, Bain S, Gross T 2002 Low-magnitude mechanical loading becomes osteogenic when rest is inserted between each load cycle. *J Bone Miner Res* **17**:1613-1619.
13. Turner CH, Owan I, Takano Y 1995 Mechanotransduction in bone: role of strain rate. *Am J Physiol* **269** (*Endocrinol Metab* **32**):E438-E442.
14. Lang T, LeBlanc A, Evans H, Lu H, Genant H, Yu A 2004 Cortical and trabecular bone mineral loss from the spine and hip in long-duration spaceflight. *J Bone Miner Res* **19**:1006-1012.
15. Collet PH, Uebelhart D, Vico L, Moro L, Hartmann D, Roth M, Alexandre C 1997 Effects of 1- and 6-month spaceflight on bone mass and biochemistry in two humans. *Bone* **20**:547-551.
16. Morey-Holton ER, Globus RK 1998 Hindlimb unloading of growing rats: a model for predicting skeletal changes during spaceflight. *Bone* **22**: 83S-88S.
17. Bloomfield SA, Allen MR, Hogan HA, Delp MD 2002 Site- and Compartment-specific changes in bone with hindlimb unloading in mature adult rats. *Bone* **31**: 149-157.
18. Vico L, Novikov VE, Very JM, Alexandre C 1991 Bone histomorphometric comparison of rat tibial metaphysis after 7-day tail suspension vs. 7-day spaceflight. *Aviat Space Environ Med* **62**:26-31.
19. Zerath E, Canon F, Guezennec CY, Holy X, Renault S, Andre C 1995 Electrical stimulation of leg muscles increases tibial trabecular bone formation in unloaded rats. *J Appl Physiol* **79**(6):1889-1894.
20. Wei CN, Ohira Y, Tanaka T, Yonemitsu H, Ueda A 1998 Does electrical stimulation of the sciatic nerve prevent suspension-induced changes in rat hindlimb bones? *Jpn J Physiol* **48**:33-37.

21. Midura RJ, Dillman CJ, Grabiner MD 2005 Low amplitude, high frequency strains imposed by electrically stimulated skeletal muscle retards the development of osteopenia in the tibia of hindlimb suspended rats. *Med Eng Phys* **27**:285-293.

22. Fluckey JD, Dupont-Versteegden EE, Montague DC, Knox M, Tesch P, Peterson CA, Gaddy-Kurten D 2002 A resistance exercise regimen attenuates losses of musculoskeletal mass during hindlimb suspension. *Acta Physiol Scand* **176**:293-300.

23. *Omega Engineering*. The Strain Gage. 1998. Omega Engineering. 11 Oct. 2005 < http://www.omega.com/literature/transactions/volume3/strain.html>.

24. Witzmann F, Kim D, Fitts R 1982 Hindlimb immobilization: length-tension and contractile properties of skeletal muscle. *J Appl Physiol* **53**:335-345.

25. Warren GL, Stallone JL, Allen MR, Bloomfield SA 2004 Functional recovery of the plantorflexor muscle group after hindlimb unloading in the rat. *Eur J Appl Physiol* **93**: 130-138.

26. Warren GL, Ingalls CP, Armstrong RB 1998 A stimulating nerve cuff for chronic in vivo measurements of torque produced about the ankle in the mouse. *J Appl Physiol* **84**:2171-2176.

# APPENDIX A

## RAW STRAIN VS. TIME PLOTS

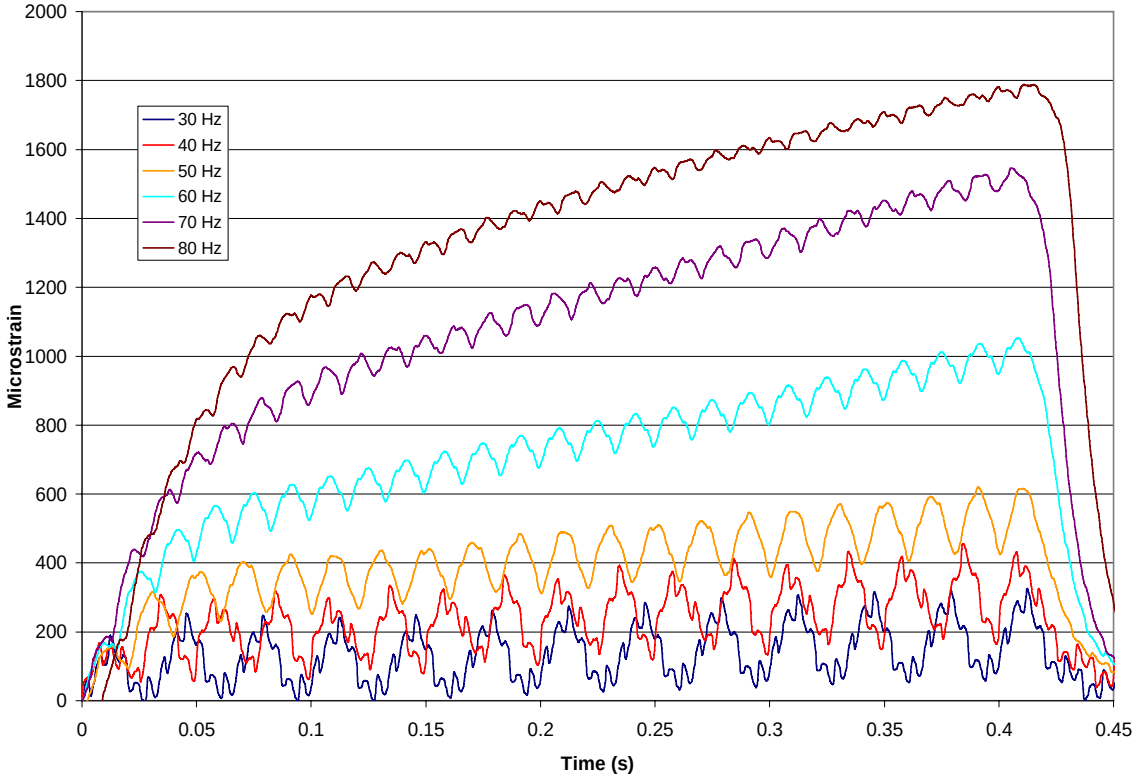


**Figure A-1.** Strain vs. time for animal number 1555.

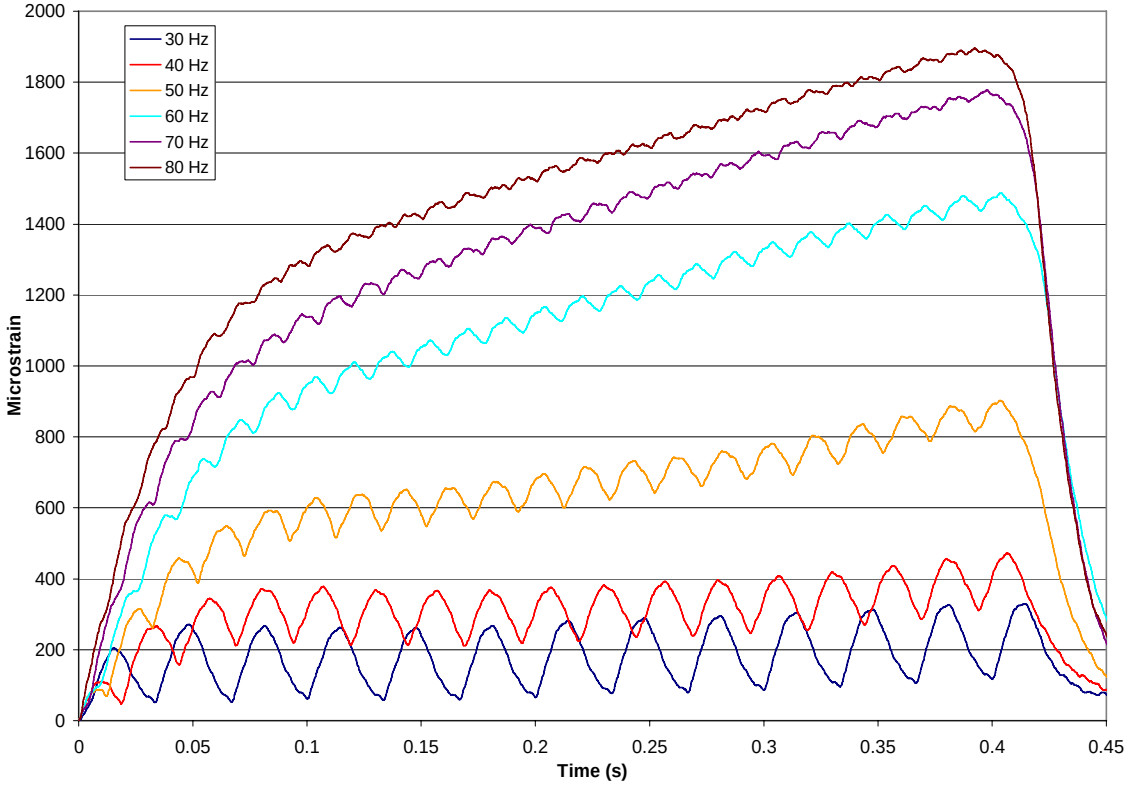


**Figure A-2.** Strain vs. time for animal number 1556.

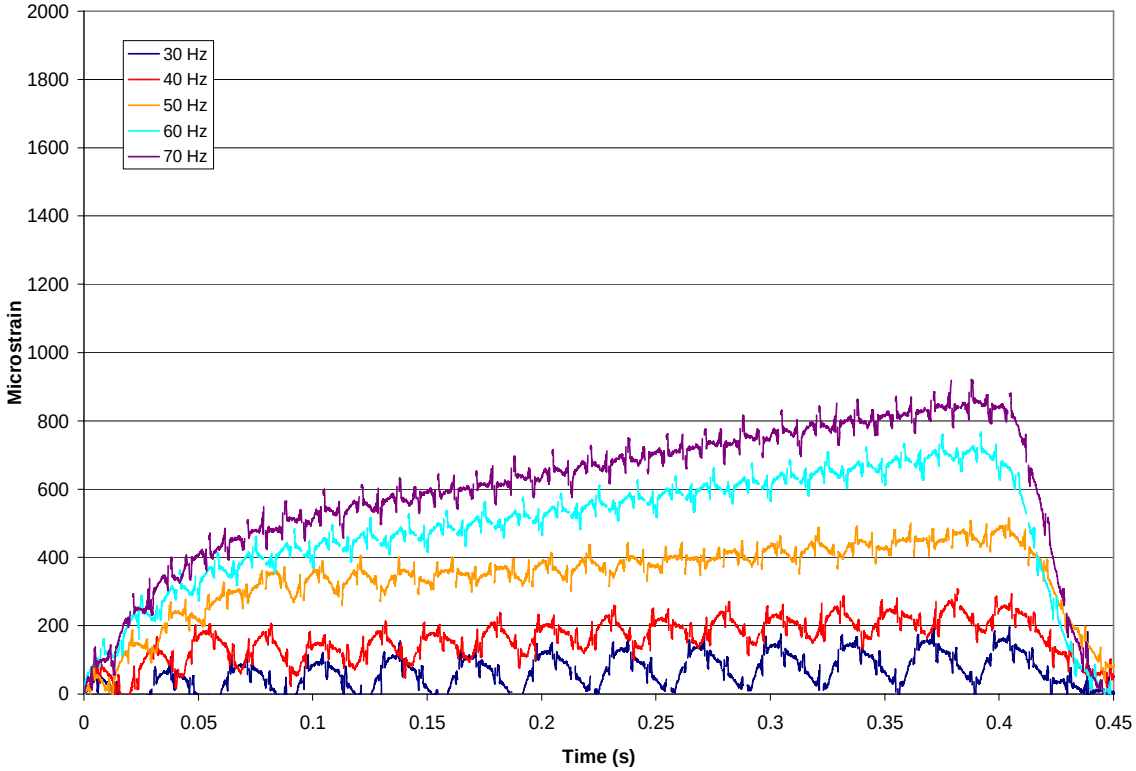


**Figure A-3.** Strain vs. time for animal number 1557.

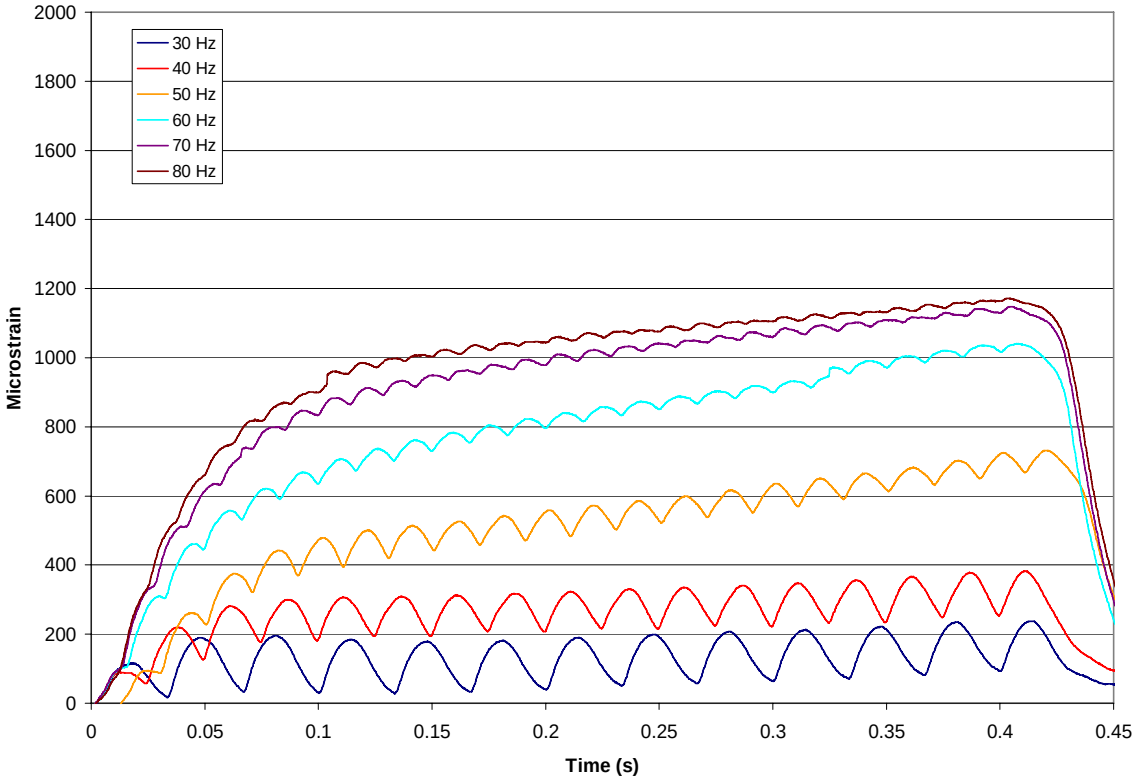


**Figure A-4.** Strain vs. time for animal number 1501.

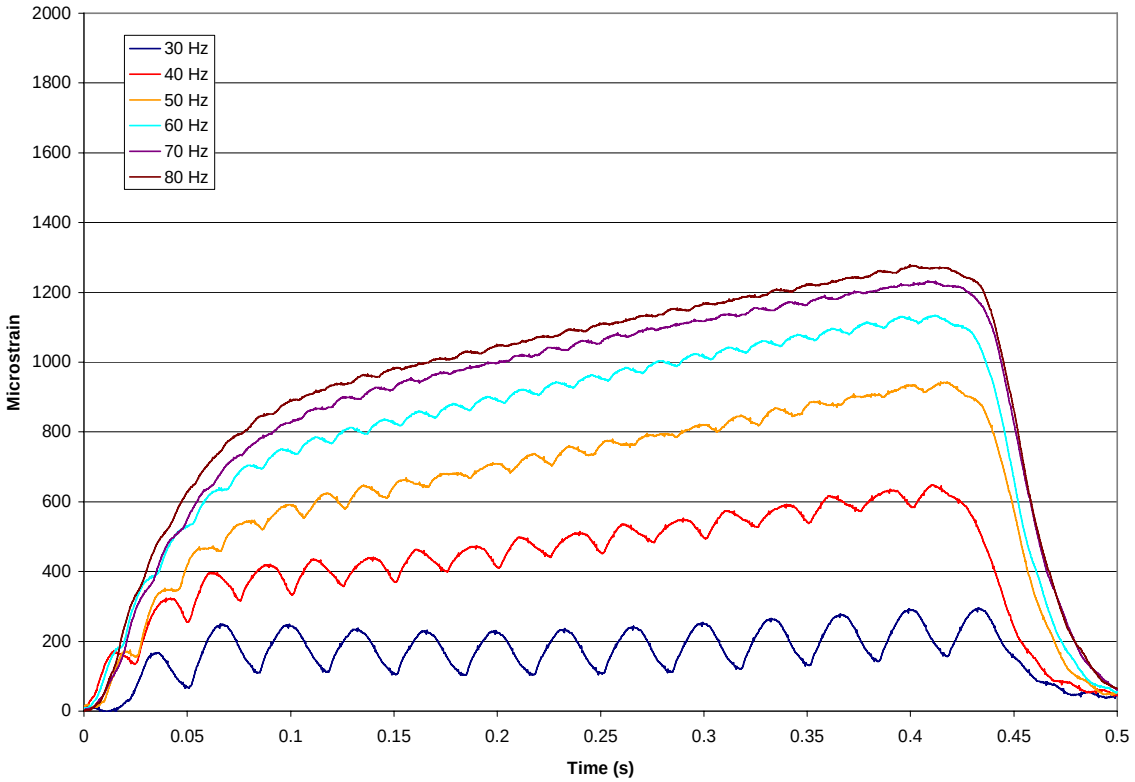


**Figure A-5.** Strain vs. time for animal number 1550.

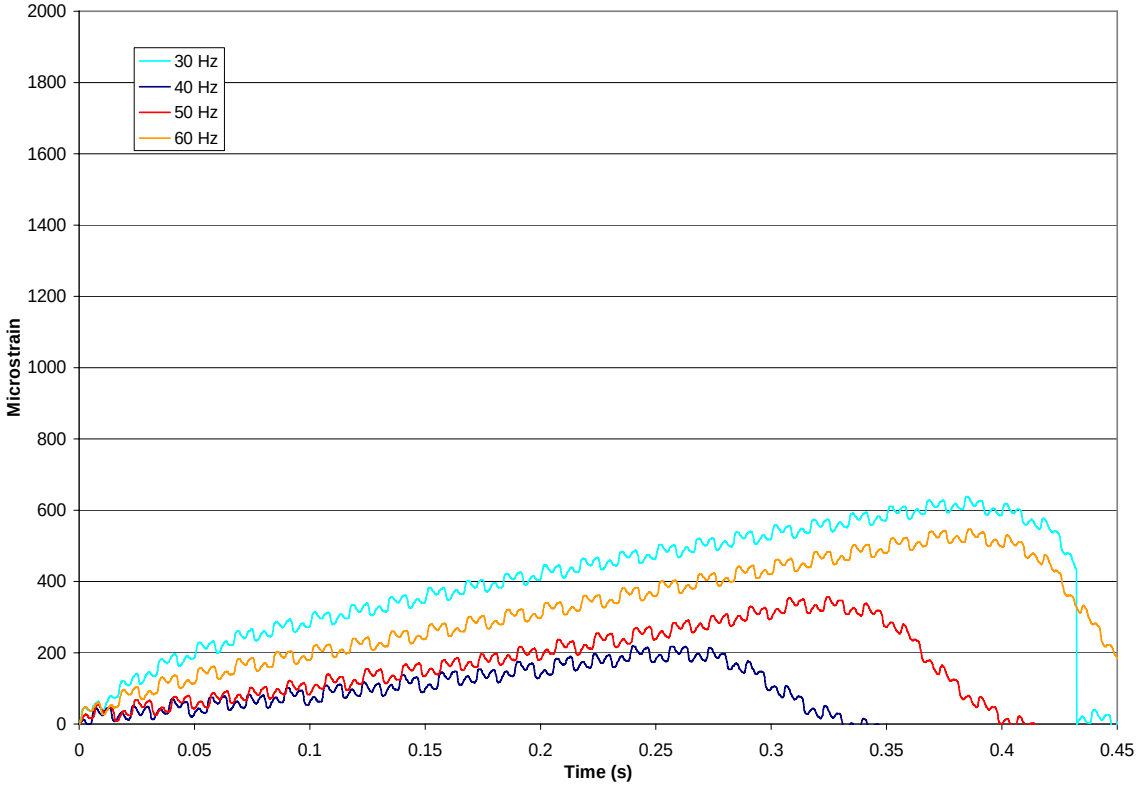


**Figure A-6.** Strain vs. time for animal number 1562.

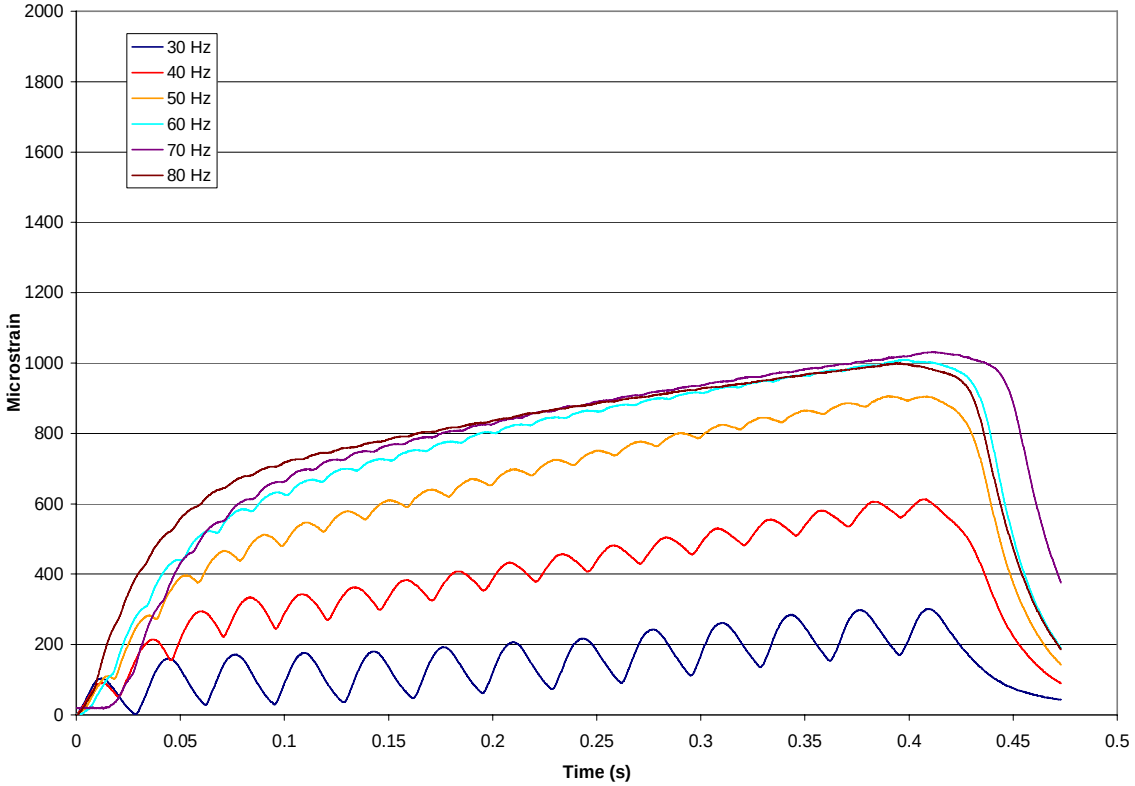


**Figure A-7.** Strain vs. time for animal number 1558.

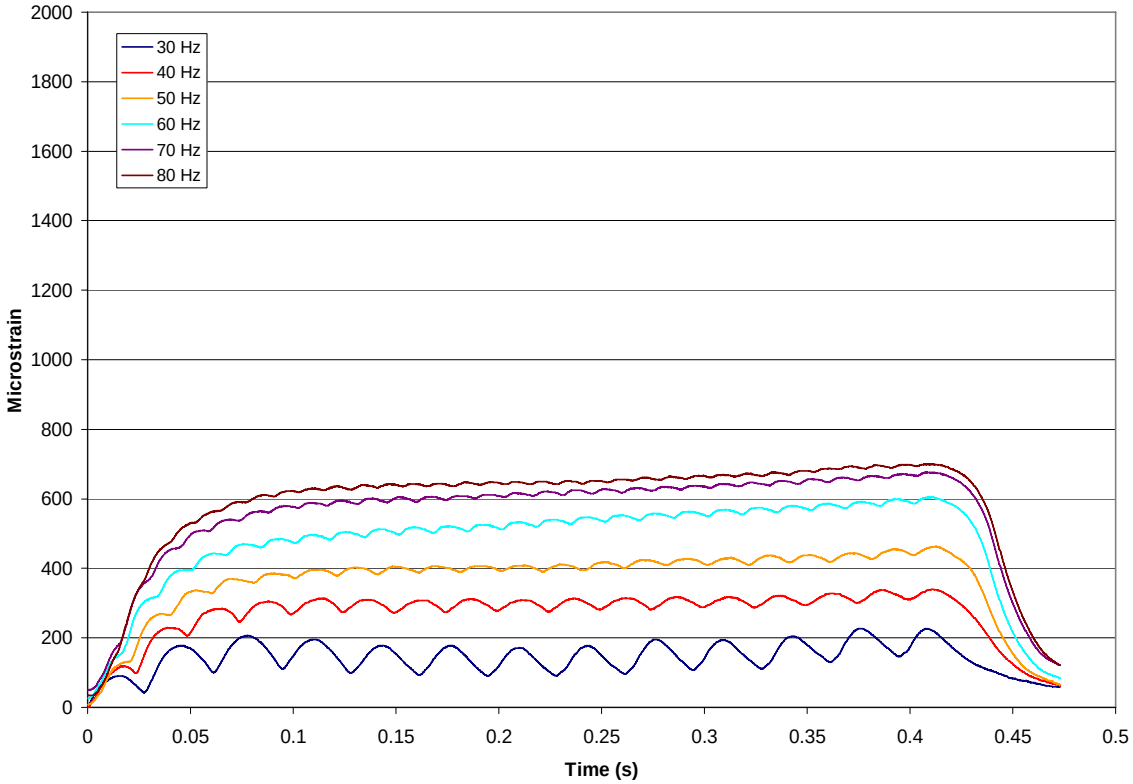


**Figure A-8.** Strain vs. time for animal number 1560.

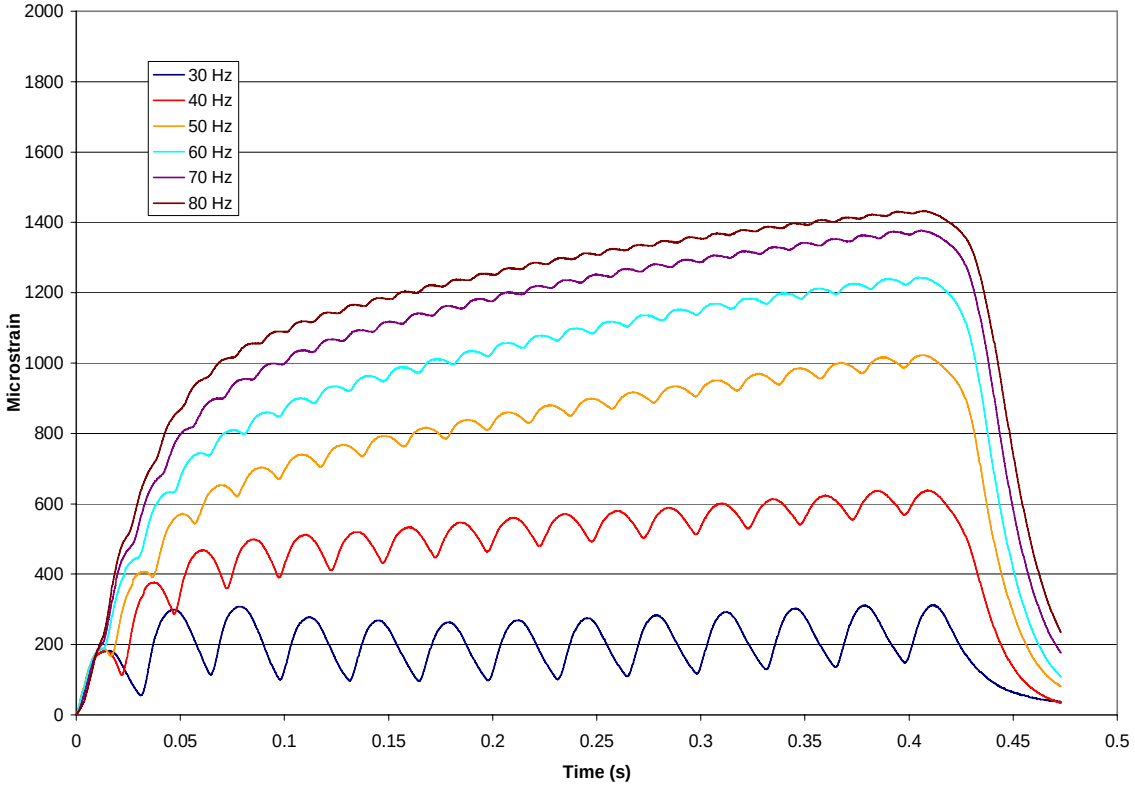


**Figure A-9.** Strain vs. time for animal number 1561.

# APPENDIX B

## TORQUE VALUES

**Table B-1**. Torque values for baseline animal strain measurements.

| BL | | | |
|---|---|---|---|
| **Animal #** | **Peak Isometric Torque (N*mm)** | **Eccentric Torque (N*mm)** | **% Peak Torque** |
| **1555** | **0.208** | 0.05 | 24.04% |
| | | 0.082 | 39.42% |
| | | 0.134 | 64.42% |
| | | 0.225 | 108.17% |
| | | 0.314 | 150.96% |
| | | 0.355 | 170.67% |
| **1556** | **0.255** | 0.088 | 34.39% |
| | | 0.138 | 54.08% |
| | | 0.237 | 93.02% |
| | | 0.365 | 143.18% |
| | | 0.426 | 166.98% |
| | | 0.447 | 175.29% |
| **1557** | **0.247** | 0.079 | 32.11% |
| | | 0.122 | 49.19% |
| | | 0.200 | 80.93% |
| | | 0.292 | 118.06% |
| | | 0.341 | 138.14% |
| | | 0.362 | 146.56% |

**Table B-2**. Torque values for 7 day animal strain measurements.

| HU-7 | | | |
|---|---|---|---|
| **Animal #** | **Peak Isometric Torque (N*mm)** | **Eccentric Torque (N*mm)** | **% Peak Torque** |
| **1501** | **0.248** | 0.088 | 35.48% |
| | | 0.148 | 59.68% |
| | | 0.258 | 104.03% |
| | | 0.354 | 142.74% |
| | | 0.384 | 154.84% |
| | | 0.391 | 157.66% |
| **1550** | **0.214** | 0.09 | 42.06% |
| | | 0.179 | 83.64% |
| | | 0.272 | 127.10% |
| | | 0.312 | 145.79% |
| | | 0.328 | 153.27% |
| | | 0.337 | 157.48% |
| **1562** | **0.139** | 0.108 | 77.59% |
| | | 0.1567 | 112.57% |
| | | 0.2 | 143.68% |
| | | 0.21 | 150.86% |
| | | * | * |
| | | * | * |

* Data were excluded because at stimulation frequencies of 70 and 80 Hz, irregular muscle contractions were observed. The animal appeared to be ill before strain measurements.

**Table B-2**. Torque values for 21 day animal strain measurements.

| HU-21 | | | |
|---|---|---|---|
| **Animal #** | **Peak Isometric Torque (N*mm)** | **Eccentric Torque (N*mm)** | **% Peak Torque** |
| **1558** | **0.211** | 0.1453 | 68.86% |
| | | 0.2783 | 131.90% |
| | | 0.3649 | 172.94% |
| | | 0.3951 | 187.25% |
| | | 0.3993 | 189.24% |
| | | 0.3987 | 188.96% |
| **1560** | **0.21** | 0.09 | 42.86% |
| | | 0.1752 | 83.43% |
| | | 0.2769 | 131.86% |
| | | 0.33 | 157.14% |
| | | 0.354 | 168.57% |
| | | 0.3604 | 171.62% |
| **1561** | **0.211** | 0.1008 | 47.77% |
| | | 0.1845 | 87.44% |
| | | 0.3054 | 144.74% |
| | | 0.3557 | 168.58% |
| | | 0.37 | 175.36% |
| | | 0.3808 | 180.47% |

# APPENDIX C

# STRAIN GAGE IMPLANTATION PROCEDURE

## *C-1. Strain Gage Preparation*

1. Solder enameled lead wires to 120 Ω two-wire strain gage (EA-06-015SE-120) (Measurements Group Inc., NC).
2. Apply coat of M Coat B (nitrile rubber) (Measurements, NC) to gage and soldered junction, after three hours, apply coat of M Coat A (polyurethane) (Measurements Group, NC) to gage and soldered junction. Allow to cure for 24 hours.
3. Roughen polymide backing with 600-grit silicon carbide sandpaper.

## *C-2. Strain Gage Implantation*

1. Anesthetize animal and make 1 cm incision over antero-medial aspect of proximal diaphysis of the tibia.
2. Remove small area of periosteum by scraping surface with a scalpel at location where gage is to be attached.
3. Swab the area with a drop of 1% epinephrine solution on a cotton swab.
4. Dry and clean area with isopropyl alcohol on a cotton swab.
5. Apply cyanoacrylate to back of gage and attach gage to bone surface with pressure for 1 minute.
6. Place animal in muscle stimulation device.
7. Zero and shunt calibrate gage.
8. Measure strain at various stimulation frequencies.

# APPENDIX D

## STIMULATION FREQUENCIES AND TORQUES FOR EXERCISE SESSIONS

**Table D-1.** Torques for 7 day animal exercise sessions.

| Animal | Session # | Voltage | Peak Isometric Torque (N*mm) | Frequency (Hz) | Eccentric Torque (N*mm) |
|---|---|---|---|---|---|
| **1501** | **1** | 4 | 0.207 | 60 | 0.248 |
| | **2** | 4 | 0.239 | 60 | 0.287 |
| | **3** | 4 | 0.230 | 60 | 0.276 |
| **1550** | **1** | 5 | 0.230 | 40 | 0.263 |
| | **2** | 7 | 0.212 | 52 | 0.256 |
| | **3** | 5 | 0.255 | 50 | 0.301 |
| **1562** | **1** | 13 | 0.173 | 30 | 0.203 |
| | **2** | 4 | 0.157 | 51 | 0.186 |
| | **3** | 8 | 0.152 | 51 | 0.178 |

**Table D-2**. Torques for 21 day animal exercise sessions.

| Animal | Session # | Voltage | Peak Isometric Torque (N*mm) | Frequency (Hz) | Eccentric Torque (N*mm) |
|---|---|---|---|---|---|
| 1558 | **1** | 8 | 0.233 | 52 | 0.282 |
| | **2** | 3 | 0.215 | 50 | 0.248 |
| | **3** | 5 | 0.232 | 52 | 0.272 |
| | **4** | 9 | 0.265 | 55 | 0.300 |
| | **5** | 12 | 0.237 | 52 | 0.278 |
| | **6** | 10 | 0.239 | 44 | 0.283 |
| | **7** | 4 | 0.240 | 50 | 0.289 |
| | **8** | 7 | 0.232 | 47 | 0.278 |
| | **9** | 5 | 0.236 | 51 | 0.282 |
| 1560 | **1** | 6 | 0.189 | 35 | 0.229 |
| | **2** | 6 | 0.224 | 50 | 0.263 |
| | **3** | 9 | 0.195 | 50 | 0.234 |
| | **4** | 11 | 0.201 | 48 | 0.243 |
| | **5** | 3 | 0.228 | 49 | 0.271 |
| | **6** | 12 | 0.244 | 54 | 0.296 |
| | **7** | 8 | 0.230 | 46 | 0.275 |
| | **8** | 13 | 0.222 | 60 | 0.266 |
| | **9** | 10 | 0.219 | 53 | 0.263 |
| 1561 | **1** | 7 | 0.241 | 48 | 0.279 |
| | **2** | 6 | 0.207 | 50 | 0.248 |
| | **3** | 8 | 0.219 | 50 | 0.263 |
| | **4** | 9 | 0.221 | 48 | 0.258 |
| | **5** | 5 | 0.220 | 50 | 0.261 |
| | **6** | 7 | 0.230 | 56 | 0.270 |
| | **7** | 8 | 0.242 | 52 | 0.291 |
| | **8** | 6 | 0.249 | 58 | 0.300 |
| | **9** | 7 | 0.251 | 56 | 0.303 |

# VITA

Name: Brent Aron Vyvial

Address: 2711 Aspen Dr.
Rosenberg, TX 77471

Email: bvyvial@neo.tamu.edu

Education: B.S., Mechanical Engineering, Texas A&M University, 2004
M.S., Mechanical Engineering, Texas A&M University, 2006

Publications: Hogan, H.A., Vyvial, B.A., Alcorn, J.D., Swift, J.M., Prisby R.D., Bloomfield, S.A., Delp, M.D., Alterations in Mechanical Properties of Bone due to Type II Diabetes, Abstract M458, 27th Annual Meeting of the American Society for Bone and Mineral Research, Sep. 23-27, 2005, Nashville, TN.

Alcorn, J.D., Hogan, H.A., Vyvial, B.A., Bloomfield, S.A., Osteogenic Effect of Electric Muscle Stimulation as a Countermeasure during Hindlimb Unloading, Abstract 51, 23rd Annual Meeting of Houston Society for Engineering in Medicine and Biology, Feb. 9-10, 2006, Houston, TX.

Awards: HSEMB Louis C. Sheppard Award for Best Poster
Robert H. Fletcher Graduate Fellowship